Article

A skeletal muscle–sympathetic nerve–intestine network underlies muscle inflammation and atrophy induced by immobilization

Yu Hirata,[1,2] Kazuhiro Nomura,[1,3] Kaori Hozumi,[1] Kenji Sugawara,[1] Yusei Hosokawa,[1] Kana Uchiyama,[1] Tomoya Inoue,[1] Tomoko Nishigaki,[1] An Liyuan,[1] Serika Yamada,[4] Yutaro Miyatake,[4] Takahiro Niikura,[5,6] Tomoaki Fukui,[5] Keisuke Oe,[5] Ryosuke Kuroda,[5] Sotaro Hamakita,[7] Shohei Kumagai,[8] Jun Hirata,[8] Gerard Karsenty,[9] Yushi Hirota,[1] Kento Ohbayashi,[10] Toshihiko Yada,[11,12,13] Kazunari Miyamichi,[4] Christopher K. Glass,[2,14] Yusaku Iwasaki,[10] and Wataru Ogawa[1,15,*]

[1]Division of Diabetes and Endocrinology, Department of Internal Medicine, Kobe University Graduate School of Medicine, Kobe, Japan
[2]Department of Cellular and Molecular Medicine, University of California San Diego, La Jolla, CA, USA
[3]Department of Nutrition and Metabolism, Institute of Biomedical Sciences, Tokushima University Graduate School, Tokushima, Japan
[4]Laboratory for Comparative Connectomics, RIKEN Center for Biosystems Dynamics Research, Kobe, Japan
[5]Department of Orthopaedic Surgery, Kobe University Graduate School of Medicine, Kobe, Japan
[6]Department of Orthopaedic Surgery, Hyogo Prefectural Nishinomiya Hospital, Hyogo, Japan
[7]R&D, Noster Inc., Kyoto, Japan
[8]Pharmaceutical Discovery Research Laboratories, Teijin Pharma Limited, Hino, Japan
[9]Department of Genetics and Development, Vagelos College of Physicians and Surgeons, Columbia University, New York, NY, USA
[10]Laboratory of Animal Science, Graduate School of Life and Environmental Sciences, Kyoto Prefectural University, Kyoto, Japan
[11]Center for Integrative Physiology, Kansai Electric Power Medical Research Institute, Kyoto, Japan
[12]Department of Diabetes, Endocrinology and Metabolism/Rheumatology and Clinical Immunology, Gifu University Graduate School of Medicine, Gifu, Japan
[13]Division of Diabetes, Metabolism and Endocrinology, Kobe University Graduate School of Medicine, Kobe, Japan

[14]Department of Medicine, University of California San Diego, La Jolla, CA, USA
[15]Lead contact
*Correspondence: ogawa@med.kobe-u.ac.jp

Abstract

Immobility is a common cause of muscle atrophy, but the underlying mechanisms have remained unclear. Here we show that limb immobilization in mice elicits inflammation and atrophy of skeletal muscle that are preventable by neutralizing antibodies to the chemokine CXCL10. Limb immobilization also induced changes to the gut microbiota and intestinal inflammation, and either sterilization of the intestine with antibiotics or administration of 10-hydroxy-*cis*-12-octadecenoic acid—a linoleic acid–derived gut microbial metabolite—prevented intestinal and muscle inflammation as well as muscle atrophy induced by immobilization, implicating intestinal inflammation in muscle inflammation and atrophy. Limb immobilization activated sympathetic nerves and increased β2-adrenergic receptor gene (*Adrb2*) expression in the intestine. Single-cell RNA-sequencing analysis revealed that, among cells expressing *Adrb2* in the intestine, immobilization increased only the population of macrophages. Pharmacological inhibition or macrophage-specific ablation of Adrb2 prevented immobilization-induced intestinal and muscle inflammation. Our results thus implicate a previously unrecognized muscle-nerve-intestine network in immobilization-induced muscle atrophy.

Keywords

Muscle atrophy, immobility, inflammation, CXCL10, gut microbiota, β2-adrenergic receptor, gut microbial metabolite, 10-hydroxy-*cis*-12-octadecenoic acid, single-cell RNA sequencing

Introduction

Muscle mass is an important determinant of human health. A reduction in muscle mass together with the consequent decline in physical performance can trigger or accelerate various pathological conditions.[1] Exercise is an important stimulus for muscle growth,[2] and immobilization is one of the most common causes of muscle mass loss.[3] The decline in muscle mass induced by immobilization is attributable at least in part to the loss of exercise stimulation.[4] However, whereas the exercise-induced increase in muscle mass generally occurs over a time span of weeks to months, immobilization elicits a more rapid decline in muscle mass, sometimes within just a few days,[5] suggesting that immobilization actively triggers mechanisms that reduce muscle mass in a manner independent of the loss of exercise-induced muscle growth. The mechanisms by which immobilization proactively induces muscle mass loss have remained unclear, however.

We recently showed that limb immobilization, either by cast-fixation or motor nerve resection, results in a decline in the basal intracellular Ca^{2+} concentration of muscle cells through downregulation of the Ca^{2+} channel Piezo1.[6] This reduction in the cytosolic Ca^{2+} level in turn promotes protein catabolism in a manner dependent on the transcription factor KLF15 and the cytokine interleukin (IL)–6. These findings suggest that an increase in protein catabolism mediated by a Piezo1/KLF15/IL-6 pathway is a key contributor to the loss of muscle mass actively triggered by immobility.[6] On the other hand, inflammatory signals have also been implicated in immobility-induced muscle atrophy,[7,8,9] although the relation between protein catabolism and inflammation during immobility has remained unclear.

To provide further insight into the mechanisms by which immobility induces muscle atrophy, we have now investigated the time-dependent changes in skeletal muscle during limb immobilization. We found that the prominent pathological effect of limb immobilization on skeletal muscle transitions from protein catabolism to inflammation in a time-dependent manner. We also found that this muscle inflammation is dependent on changes to the gut microbiota and on intestinal inflammation triggered by the activation of sympathetic nerves in the intestine.

Results

Transition from protein catabolism to inflammation during skeletal muscle immobilization

We previously showed that limb immobilization for a relative short period (up to 3 days) induced by either cast-fixation or motor nerve resection results in a decline in skeletal muscle mass through an increase in protein catabolism mediated by a

Piezo1/KLF15/IL-6 axis.[6] We here investigated how more prolonged limb immobilization affects skeletal muscle. Cast-fixation of the hind limbs of mice resulted in a significant reduction in muscle mass of the immobilized limbs within the first 3 days of immobilization, and this decline in muscle mass continued thereafter in a time-dependent manner (Figure 1A). Prolonged immobilization did not affect food intake, body mass, or epididymal white adipose tissue (eWAT) mass (Figures S1A–S1C). The progression of muscle fiber atrophy during immobilization was confirmed by a decrease in muscle fiber area detected by histological analysis (Figures 1B and 1C, Figures S1D and S1E). The decrease in fiber area was observed in both slow- and fast-twitch fibers (Figures S1F and S1G). Immunohistochemical staining revealed that limb immobilization for 10 days, but not that for 3 days, resulted in a significant accumulation of cells positive for the macrophage marker F4/80 in the affected muscle (Figures 1B and 1D, Figures S1D and S1H). Flow cytometry also revealed an increase in the proportion of $CD11b^{+}F4/80^{+}$ cells among $CD45^{+}Ly6G^{-}$ cells in muscle (Figures 1E and 1F), and that the percentages of $CD11c^{+}CD206^{-}$ and $CD11c^{-}CD206^{+}$ cells among these $CD11b^{+}F4/80^{+}$ cells were increased and decreased, respectively, after limb immobilization for 10 days (Figures S2A–S2C). These results thus indicated that limb immobilization for 10 days induced the accumulation of macrophages in skeletal muscle as well as increased and decreased the proportions of pro-inflammatory and anti-inflammatory subsets of these cells, respectively.

Reverse transcription and quantitative polymerase chain reaction (RT-qPCR) analysis revealed that the expression of genes related to protein catabolism was upregulated in immobilized muscle, peaking at 1 to 3 days (Figure 1G and Figure S2D), consistent with our previous findings.[6] In contrast, the expression of genes related to inflammation was significantly upregulated during a later phase of immobilization, peaking at 10 days (Figure 1G and Figure S2D). RNA–sequencing (seq) analysis of immobilized muscle indicated that genes related to the proteasome, protein processing in the endoplasmic reticulum (ER), mitophagy, and autophagy were upregulated at 3 days (Figure 1H), whereas those related to cytokine–cytokine receptor interaction, hematopoietic cell lineage, phagosome, and chemokine signaling pathway were upregulated after immobilization for 10 days (Figure 1I). Gene set enrichment analysis (GSEA) also confirmed the upregulation of genes related to the proteasome or to cytokine–cytokine receptor interaction after 3 and 10 days of immobilization, respectively (Figures S2E and S2F).

Hind limb immobilization induced by motor nerve denervation similarly resulted in a time-dependent decline in skeletal muscle mass that was associated with

136 the upregulation of genes related to protein catabolism or to inflammation at 3 and 10
137 days, respectively, as well as with the accumulation of F4/80-positive cells at 10 days
138 (Figure S3). Together, these results thus revealed a transition from protein catabolism to
139 inflammation during muscle atrophy triggered by prolonged limb immobilization.
140
141 **CXCL10 mediates inflammation and atrophy of muscle induced by immobilization**
142 We next attempted to identify a humoral factor that might contribute to muscle
143 inflammation during limb immobilization. RNA-seq analysis indicated that the gene for
144 the chemokine CXCL10 was one of the most markedly induced inflammatory humoral
145 factor genes in skeletal muscle under this condition (Figures 2A and 2B). The
146 expression of *Cxcl10* was increased 1 day after the onset of limb immobilization by
147 cast-fixation, peaked at 7 days, and decreased thereafter (Figure 2C). The circulating
148 (Figure 2D) and muscle (Figure S4A) concentration of CXCL10 was similarly increased
149 during limb immobilization. The upregulation of *Cxcl10* expression was apparent in
150 both the blood cell and non–blood cell fractions of muscle, which were discriminated on
151 the basis of the expression of CD45 (Figure S4B); however, it was more pronounced in
152 the non–blood cell fraction, which was composed mostly of myofibers. These results,
153 along with the finding that CXCL10 concentrations in muscle tissue were
154 approximately ten times greater than those in circulation (Figure 2D and Figure S4A),
155 suggest that the cytokine acts in an autocrine/paracrine manner. Moreover, a similar
156 increase in *Cxcl10* expression was also detected in skeletal muscle of denervated mice
157 (Figure S4C). Of note, upregulation of the CXCL10 gene (Figure 2E) and of other
158 inflammation-related genes (Figure S4D) was observed in human skeletal muscle after
159 cast-fixation for an average of 8.3 ± 3.1 days as a result of bone fractures. Furthermore,
160 analysis of publicly available human gene expression data revealed that acute
161 immobilization of lower limbs was associated with an increase in the abundance of
162 *CXCL10* mRNA in skeletal muscle (Figure S4E).
163 The administration of neutralizing antibodies to CXCL10 inhibited both the
164 accumulation of macrophages (Figures 2F and 2G) and the upregulation of
165 inflammation-related gene expression (Figure 2H) in muscle during subsequent limb
166 immobilization by cast-fixation. These antibodies also attenuated the decrease in both
167 skeletal muscle mass (Figure 2I) and muscle fiber area (Figures 2F and 2J) induced by
168 prolonged limb immobilization. Immobilization increased the phosphorylation of ERK,
169 a signaling molecule activated by CXCL10,[10] in the gastrocnemius muscle, which was
170 prevented by the neutralizing antibodies (Figure S5A). These results suggest that the
171 antibodies indeed attenuated CXCL10-mediated signaling in muscle. The neutralizing

172 antibodies to CXCL10 did not affect the upregulation of catabolism-related genes or the
173 decline in muscle mass apparent after limb immobilization for 3 days (Figures S5B and
174 S5C).
175 Collectively, these findings suggested that inflammation mediated by CXCL10
176 plays a key role in the loss of muscle mass induced by immobilization, whereas protein
177 catabolism, which is activated relatively early during immobilization, is independent of
178 this CXCL10 pathway.
179
180 **Prolonged limb immobilization induces inflammation in the intestine**
181 Given that prolonged limb immobilization gives rise to inflammation in skeletal muscle,
182 we next explored whether such immobilization also induces inflammation in other
183 organs. Examination of the entire body of cast-immobilized mice revealed intestinal
184 shortening (Figures 3A and 3B), a decrease in cecum mass (Figure 3C), and a reduction
185 in the depth of crypts in the colon (Figures 3D and 3E), all of which are associated with
186 intestinal inflammation.[11] A decrease in tissue mass was also apparent for the small and
187 large intestine, but not for the stomach or duodenum (Figure S6A). The reduction in the
188 length of the small and large intestine as well as that in cecum mass became evident
189 within 7 to 10 days of the onset of limb immobilization (Figures S6B and S6C),
190 showing a time course similar to that of skeletal muscle inflammation.
191 Immunohistochemical analysis and flow cytometry revealed that prolonged limb
192 immobilization resulted in the accumulation of F4/80-positive cells and
193 $CD11b^{+}F4/80^{+}$ cells, respectively, in the intestinal wall (Figures 3D and F–H), with a
194 concomitant increase in the proportion of pro-inflammatory ($CD11c^{+}CD206^{-}$) and
195 decrease in that of anti-inflammatory ($CD11c^{-}CD206^{+}$) macrophages (Figures S7A–
196 S7C). In addition, RT-qPCR analysis showed that the expression of inflammation-
197 related genes, was upregulated in the distal small intestine and colon, but not in the
198 proximal small intestine, of mice subjected to cast-fixation for 10 days (Figure S8A).
199 Cast-fixation did not upregulate *Cxcl10* in the small or large intestine (Figure S8B).
200 GSEA of RNA-seq data obtained from the intestine of such mice revealed upregulation
201 of genes related to inflammation, including those associated with cytokine and
202 chemokine signaling pathways (Figure 3I). Denervation-induced limb immobilization
203 for 10 days also resulted in intestinal shortening (Figure S8C), a decrease in cecum
204 mass (Figure S8D), and upregulation of inflammation-related genes in the distal small
205 intestine and colon (Figure S8E).
206 Intestinal inflammation is typically associated with impairment of the intestinal
207 barrier, resulting in an increase in the circulating levels of bacterial components such as

208 lipopolysaccharide (LPS).[12] Consistent with this scenario, prolonged limb
209 immobilization resulted in a decrease in the intestinal abundance of claudin-1 (Figure
210 3J), a key protein in maintenance of the intestinal barrier,[13] and in an increase in the
211 plasma concentration of LPS (Figure 3K). Furthermore, treatment of cultured C2C12
212 myotubes with LPS resulted in the upregulation of *Cxcl10* expression (Figure 3L).
213 Collectively, these results suggested that prolonged limb immobilization triggers
214 intestinal inflammation, which may then contribute to upregulation of CXCL10
215 expression and consequent induction of inflammation in skeletal muscle. Given the
216 increase in plasma LPS concentration, we analyzed the effect of hindlimb
217 immobilization on other skeletal muscles, including forelimb muscles (flexor carpi
218 ulnaris) and diaphragm. Whereas the mRNA abundance of *Il1b* was increased (Figure
219 S9A), the expression of *Cxcl10* (Figure S9A), as well as the mass (Figure S9B) of these
220 muscles, remained unaltered, suggesting that inflammation occurred systemically, but
221 another factor induced in immobilized muscles is required for the upregulation of
222 *Cxcl10* and muscle atrophy. In addition, RNA-seq analysis of the forelimb muscles
223 showed the upregulation of genes related to muscle contraction, exercise, and amino
224 acid metabolism (Figure S9C), suggesting that hindlimb immobilization may induce a
225 compensatory response in the forelimb muscles.
226
227 **The gut microbiota contributes to inflammation and atrophy of skeletal muscle**
228 **induced by limb immobilization**
229 The development of intestinal inflammation is closely related to changes in the gut
230 microbiota.[12] We therefore investigated the impact of prolonged limb immobilization on
231 the gut microbiota. Analysis of bacterial 16S rRNA genes revealed that prolonged
232 immobilization of the hind limbs of mice by cast-fixation resulted in marked changes to
233 the gut microbiota including an increase in the abundance of the Lachnospiraceae group
234 and a decrease in that of *Lactobacillus* species (Figures 4A and 4B). These changes in
235 the gut microbiota were also demonstrated by principal coordinate analysis (Figure 4C),
236 and they were largely reversed within 2 weeks after cast removal (Figures S10A–S10C),
237 indicating that the changes were indeed primarily triggered by limb immobilization.
238 Furthermore, limb immobilization by motor nerve denervation resulted in changes to
239 the gut microbiota similar to those induced by cast-fixation (Figures S10D and S10E).
240 Fecal microbiota transplantation from non–cast-immobilized control mice into
241 cast-immobilized mice attenuated colon and skeletal muscle inflammation and mitigated
242 the loss of muscle mass induced by cast-fixation (Figures 4D–4F). Pseudosterilization
243 of the intestine by oral administration of antibiotics also attenuated muscle

244 inflammation and atrophy induced by cast-fixation (Figures S11A and S11B).
245 Furthermore, intrarectal administration of clodronate liposomes inhibited the
246 accumulation of macrophages in the colon (Figure 4G), and attenuated the upregulation
247 of inflammation-related genes in muscle and the decrease in muscle mass induced by
248 immobilization (Figures 4H and 4I).
249 These results thus implicate that alterations in the gut microbiota and intestinal
250 macrophage activation play a critical role in mediating skeletal muscle inflammation
251 and atrophy induced by prolonged limb immobilization.
252
253 **A gut microbial metabolite derived from linoleic acid inhibits intestinal and muscle**
254 **inflammation as well as muscle atrophy induced by limb immobilization**
255 We next examined whether the prevention of intestinal inflammation might ameliorate
256 the loss of skeletal muscle induced by prolonged limb immobilization. We focused on
257 gut microbial metabolites derived from linoleic acid (LA), which have been shown to
258 exert various biological effects including the prevention of drug-induced colitis.[14-16]
259 Analysis of various LA-derived fatty acid metabolites (Figure S12A) in feces by mass
260 spectrometry revealed that limb immobilization by cast-fixation for 10 days reduced the
261 abundance of LA and 13-hydroxy-*cis*-9-octadecenoic acid (HYD) and that limb
262 denervation for 10 days reduced that of HYD and 10-hydroxy-*cis*-12-octadecenoic acid
263 (HYA) as well as that of metabolites derived from these two fatty acids including 13-
264 oxo-*cis*-9-octadecenoic acid (KetoD), 10,13-dihydroxy-octadecanoic acid (HYE), 10-
265 oxo-*cis*-12-octadecenoic acid (KetoA), and 10-oxo-*trans*-11-octadecenoic acid (KetoC)
266 (Figures S12B and S13A), indicating that limb immobilization altered LA metabolism
267 in the intestine.
268 Given that the abundance of LA, together with that of HYA and HYD, both of
269 which are directly derived from LA, was decreased during limb immobilization, we fed
270 mice with normal chow or chow containing these fatty acids for 10 days and then
271 subjected them to limb immobilization. Dietary supplementation with LA or either of
272 the LA metabolites did not influence chow intake (Figure S13B). Oral administration of
273 HYA, but not that of LA or HYD, attenuated the reduction in crypt depth and the
274 accumulation of F4/80-positive cells in the colon (Figures 5A–5C) as well as the
275 shortening of the colon (Figure S14A) induced by cast-fixation. Furthermore, treatment
276 with HYA inhibited the upregulation of inflammation-related gene expression (Figure
277 S14B) and the downregulation of claudin-1 protein (Figure S14C) in the colon triggered
278 by prolonged limb immobilization. Gene ontology (GO) analysis of RNA-seq data for
279 the colon revealed that the top 20 processes enriched among genes whose expression

280 was upregulated by immobilization include various inflammatory cell–related categories
281 (Figure S15A) and that treatment of limb-immobilized mice with HYA attenuated the
282 expression of genes in these categories (Figure S15B). In addition, HYA, but not LA or
283 HYD, prevented the immobilization-induced increase in the plasma concentration of
284 LPS (Figure S15C).
285 Oral administration of HYA, but not that of LA or HYD, also attenuated the
286 decline in muscle mass (Figure 5D) as well as the reduction in muscle fiber area and the
287 accumulation of F4/80-positive cells in soleus muscle (Figure 5E, Figures S16A and
288 S16B) induced by limb immobilization. Furthermore, HYA treatment suppressed the
289 immobilization-induced upregulation of inflammation-related gene expression in
290 skeletal muscle (Figure S16C) while the changes in the gut microbiota caused by
291 immobilization was unaltered by this treatment (Figure S16D). Together, these data
292 indicated that oral administration of HYA ameliorated intestinal inflammation
293 independently of improving dysbiosis, which in turn resulted in attenuation of
294 inflammation and atrophy of skeletal muscle, in mice subjected to limb immobilization.
295
296 **Sympathetic nerve activation contributes to intestinal inflammation induced by**
297 **limb immobilization**
298 We next investigated the mechanism by which limb immobilization triggers intestinal
299 inflammation. We examined the possible role of the nervous system—in particular, the
300 sympathetic nervous system—given that sympathetic nerves regulate immune responses
301 in various tissues including the intestine.[17,18]
302 Given that tissue catecholamine concentrations do not necessarily reflect
303 sympathetic neuronal activity, we first assessed norepinephrine (NE) turnover, which is
304 commonly used as an index of sympathetic nerve-related catecholamine dynamics.[19,20]
305 The NE content of tissue was thus determined before and after the intraperitoneal
306 administration of α-methyl-*p*-tyrosine (α-MT), an inhibitor of catecholamine synthesis.
307 As expected, α-MT treatment reduced NE content in all parts of the digestive tract
308 examined (Figure 6A). Whereas the extent of the decrease in NE content induced by α-
309 MT was similar for the stomach and the duodenum between control mice and mice
310 subjected to cast-immobilization for 10 days, that for the proximal or distal small
311 intestine or for the colon was greater in immobilized mice (Figures 6A and 6B),
312 indicating that NE turnover was selectively augmented in the lower intestine of the
313 immobilized animals. We also evaluated the levels of NE and its primary metabolite,
314 DHPG (3,4-dihydroxyphenylglycol) simultaneously to assess NE dynamics, and found
315 that the DHPG/NE ratio was markedly increased in the intestinal tissues, except for the

316 stomach, in immobilized mice (Figure S17A), suggesting enhanced norepinephrine
317 metabolic dynamics in the lower intestine of immobilized mice.
318 To test the functional involvement of sympathetic nerves, we performed
319 chemical sympathectomy using 6-hydroxydopamine (6-OHDA). 6-OHDA treatment
320 reduced NE content of the intestinal tissues (Figure 6C) and inhibited the increase in the
321 proportion of pro-inflammatory macrophages in the colon and the increase in the
322 abundance of the Lachnospiraceae group, as well as the decline in skeletal muscle mass
323 induced by immobilization (Figures 6D–6H). In addition, we selectively activated
324 sympathetic neurons projecting to intestinal tissues by targeting *Cartpt*-expressing
325 spinal sympathetic preganglionic neurons, which were recently shown to project
326 selectively to the intestine.[21] Mice with intestinal tissue-specific sympathetic nerve
327 activation showed the upregulation of inflammation-related genes in the colon and a
328 tendency toward reduced skeletal muscle mass (Figures 6I and 6J). These results thus
329 indicated that activation of sympathetic nerves that selectively project to intestinal
330 tissues contributes to intestinal inflammation, dysbiosis, and muscle atrophy induced by
331 limb immobilization.
332 RNA-seq analysis of the colon revealed that, among genes encoding adrenergic
333 receptors, the gene for the β2-adrenergic receptor (*Adrb2*) was most markedly
334 upregulated by limb immobilization, and this upregulation was attenuated by dietary
335 intake of HYA (Figure 7A). Expression of the gene for the α2a-adrenergic receptor
336 (*Adra2a*) showed a similar pattern of changes, albeit to a lesser extent compared with
337 the changes apparent for *Adrb2* expression. Treatment of mice with α-MT or the β2-
338 adrenergic receptor antagonist propranolol, but not that with the α-adrenergic receptor
339 antagonist phentolamine, inhibited the upregulation of inflammation-related genes in
340 the intestine (Figure 7B) and skeletal muscle (Figure S17B). Furthermore, treatment of
341 mice with the β2-adrenergic receptor agonist clenbuterol induced alterations in the gut
342 microbiota that closely resembled those observed under cast immobilization (Figures
343 7C–7E). These results suggested that sympathetic nerve activation contributes to
344 immobilization-induced dysbiosis and inflammation of the intestine and skeletal muscle
345 via the activation of Adrb2 signaling. Treatment with propranolol or α-MT did not affect
346 immobilization-induced muscle atrophy, however (Figure S17C). Given that Adrb2 in
347 myofibers plays an important role in muscle hypertrophy,[22,23] an antiatrophic effect of
348 these inhibitors mediated by attenuation of Adrb2 signaling in the intestine might have
349 been counteracted by an antihypertrophic effect mediated by attenuation of Adrb2
350 signaling in muscle.

To identify cell types that mediate Adrb2 signaling in the intestine, we performed single-cell (sc) RNA-seq analysis of the colon. The single-cell fixed RNA profiling method[24] allowed us to concomitantly analyze various cell types—including epithelial, stromal, and immune cells—while maintaining their transcriptional characteristics, leading to the identification of 37 cell clusters (Figures 7F and Figure S17D). Genes that characterize each cell cluster are listed in Table S1. Cast-immobilization of hind limbs for 10 days increased the population size for various immune cell clusters including all four macrophage clusters, a macrophage/dendritic cell cluster, a dendritic cell cluster, a B cell/IgA plasma cell cluster, an IgA plasma cell cluster, and one of the two T cell clusters (Figure 7G).

Adrb2 mRNA was most abundant in two of the macrophage clusters (Macrophage_1 and Macrophage_2), one of the two B cell clusters (B cell_2), and a lymphatic endothelial cell cluster (Figure 7H and Figure S18). Among these cell types, only the population of macrophages was increased in response to limb immobilization (Figure 7G). We therefore focused on this cell type and generated macrophage-specific Adrb2 knockout (Mφ-Adrb2KO) mice. The immobilization-induced increase in population size was attenuated for three of the four macrophages clusters (Macrophage_2, _3, and _4), which express *Itgam* (Cd11b), *Fcer1g*, or *Cd14* and therefore likely correspond to pro-inflammatory macrophages, in Mφ-Adrb2KO mice (Figure 8A and Table S1). In contrast, *Adrb2* ablation increased the population size for the Macrophage_1 cluster, which expresses the anti-inflammatory macrophage markers *Cd163* and *Mrc1*,[25] in the colon of mice subjected to limb immobilization (Figure 8A and Table S1). Consistent with these findings, flow cytometry revealed that the limb immobilization–induced increase in the abundance of pro-inflammatory macrophages in the colon was prevented in Mφ-Adrb2KO mice (Figures 8B and 8C, Figures S19A and S19B). Moreover, the reduction in crypt depth and the accumulation of F4/80-positive cells (Figures 8D–8F) as well as the upregulation of *Ccl2* expression (Figure S19C) in the colon induced by limb immobilization were also all attenuated in Mφ-Adrb2KO mice.

The accumulation of macrophages and the increase in the proportion of pro-inflammatory macrophages in skeletal muscle induced by prolonged limb immobilization were also inhibited, whereas the decrease in the proportion of anti-inflammatory macrophages was unaffected, in Mφ-Adrb2KO mice (Figure 8G, Figures S19D–S19F). The decline in skeletal muscle mass induced by immobilization tended to be attenuated in Mφ-Adrb2KO mice (Figure 8H). Collectively, these results suggested

386 that Adrb2 signaling in intestinal macrophages plays a key role in skeletal muscle
387 inflammation induced by limb immobilization.
388
389 **Discussion**
390 We have here shown that the pathology of skeletal muscle associated with limb
391 immobilization transitions from catabolism to inflammation, with the latter process
392 being regulated by CXCL10 (Figure 8I). Limb immobilization results in changes to the
393 gut microbiota and intestinal inflammation that subsequently contribute to the
394 development of muscle inflammation. Furthermore, the onset of intestinal inflammation
395 is triggered by sympathetic nerve activation and Adrb2 signaling in macrophages. Our
396 results have thus uncovered a muscle-neural-intestinal network that underlies the
397 development of muscle atrophy in response to limb immobilization.
398 Whereas changes to the intestinal environment contribute to various
399 physiological and pathological processes,[26,27] our finding that limb immobilization for a
400 relatively short time (~10 days) altered the gut microbiota and intestinal environment
401 was unexpected. Our observation that the release of immobilization returned the gut
402 microbiota to its original state indicates that the initial effect was primarily induced by
403 immobilization via an intrinsic mechanism. Whereas extrinsic factors, including the
404 ingestion of food or drugs, influence the gut microbiota, little is known about the
405 intrinsic mechanisms by which the host modulates the gut microbial population. In
406 addition to its effects on immune cell clusters, limb immobilization increased the
407 population size for a progenitor cell cluster, a tuft cell cluster, two of the seven
408 fibroblast-like cell clusters (FB like cells_3 and _6), a mesothelial cell cluster, one of
409 the two enteroendocrine cell clusters (Enteroendocrine cell_1), and an enteric neuron
410 cluster in the intestine. Changes in population size and function of these cell clusters
411 may also have contributed to the immobilization-induced alterations in the intestinal
412 environment and gut microbiota.
413 Metabolites produced by the gut microbiota play an important role in symbiosis
414 with the host. HYA is a recently discovered LA-derived metabolite produced by gut
415 bacteria and has been detected in human plasma.[14] Whereas the roles of HYA and its
416 related lipid metabolites in the maintenance of human physiological functions are not
417 yet fully understood, evidence suggests that exogenous HYA administration may
418 ameliorate various pathological conditions including chemical colitis, atopic dermatitis,
419 fatty liver disease, and obesity-induced insulin resistance.[28-31] The mechanisms by
420 which HYA exerts such beneficial effects on these conditions, as well as on
421 immobilization-induced muscle inflammation, remain unclear. However, HYA not only

422 attenuates impairment of the intestinal barrier but also interacts with several host
423 proteins including fatty acid receptors.[28] Further elucidation of the detailed mechanisms
424 of HYA action may contribute to the development of its clinical use.
425 Sympathetic nerves together with immune cells that express adrenergic
426 receptors in the intestine have been implicated in the regulation of tissue damage and
427 repair.[17,18] Adrb1 and Adrb2 expressed in innate lymphoid cells of the small intestine
428 contribute to protection of the tissue against inflammation[32] and to tissue regeneration.[33]
429 The T cell_2 cluster in our analysis appears to correspond to innate lymphoid cells, with
430 the population size for this cell cluster being decreased by limb immobilization.
431 Macrophages that reside in the muscular layer of the intestine exert tissue-protective
432 actions dependent on Adrb2 signaling during bacterial infection.[34,35] We have now
433 shown that *Adrb2* was highly expressed in the Macrophage_1 and _2 clusters, which
434 manifested transcriptional characteristics of anti-inflammatory and pro-inflammatory
435 macrophages, respectively. Macrophage_1 cells therefore likely correspond to
436 macrophages that reside in the muscular layer of the intestine.
437 Our findings have potential implications for drug development. Given that the
438 safety of HYA administration in humans has been established, we have initiated a
439 clinical trial of such treatment for individuals prone to the development of muscle
440 atrophy as a result of limb immobilization after orthopedic surgery (clinical trial
441 number: jRCT2051230197). Whereas antibodies to CXCL10 have been shown to be
442 effective for the treatment of inflammatory and cardiovascular conditions in preclinical
443 studies,[36-38] a preventive effect of these antibodies on muscle atrophy has not been
444 reported. Whereas several clinical trials of agents that target CXCL10 have been
445 conducted,[39,40] such agents have yet to be introduced into clinical practice. Given that
446 the upregulation of *CXCL10* expression in muscle was associated with acute limb
447 immobilization not only in the human cohort of the present study but also in a publicly
448 available data set, clinical trials to explore the potential preventive effect of antibodies
449 to CXCL10 on immobilization-induced muscle atrophy are warranted.
450 In conclusion, our study has revealed a previously unrecognized organ-organ
451 interaction that plays a key role in the development of immobilization-induced muscle
452 atrophy. Two different interventions, both of which are immediately applicable to
453 clinical trials, were shown to be effective for prevention of this condition: the targeting
454 of muscle inflammation with antibodies to CXCL10, and that of intestinal inflammation
455 with HYA. The mechanisms by which limb immobilization signals to the sympathetic
456 nervous system and by which Adrb2 signaling in macrophages induces intestinal
457 inflammation remain to be elucidated. The characterization of these mechanisms may

contribute to the further development of new and improved treatments for muscle atrophy.

Acknowledgments

We thank Akira Suzuki for providing *LysM-Cre* mice, Hidenori Shimizu for gut microbiota analysis, and Chikako Aoki and Yoshika Ogawa for technical assistance. We also thank Mashito Sakai for the insightful discussions. This study was supported in part by grants from Japan Society for the Promotion of Science (KAKENHI grant 22K16397 to Y. Hirata) and Japan Agency for Medical Research and Development (AMED) Practical Research Project for Life-Style related Diseases including Cardiovascular Diseases and Diabetes Mellitus (Grant Number JP23ek0210192 to Y. Hirata, K.N., and W.O.), as well as by grants from Uehara Memorial Foundation, Nakatomi Foundation, Japan Society for the Study of Obesity, Center for Medical Transformation, Manpei Suzuki Diabetes Foundation, and Cell Science Research Foundation (all to Y. Hirata), and from Takeda Science Foundation (to W.O.).

Author Contributions

Y. Hirata, K.N., and W.O. conceived the study and analyzed the data. K.H., Y. Hosokawa, K.U., T.I., T. Nishigaki, A.L., S.Y., Y.M., and K.M. contributed to animal and cell experiments. K.S. contributed to analysis of the public data set. T. Niikura, T.F., K. Oe, R.K., and Y. Hirota contributed to analysis of human skeletal muscle. S.H. contributed to gut microbiota and metabolome analysis. S.K. and J.H. contributed to RNA-seq analysis. G.K. contributed to the generation of genetically engineered mice. K. Ohbayashi, T.Y., and Y.I. contributed to measurement of NE turnover. C.K.G. provided additional experimental guidance. Y. Hirata and W.O. wrote the manuscript.

Declaration of interests

W.O. has received funding from Noster for a clinical trial and has received a lecture fee from Teijin Pharma.

Supplemental information

Document S1. Figures S1–S20 and Tables S1–S3

491 **Methods**

492 **Animals**

493 *Adrb2*-floxed mice were described previously,[41] and *LysM-Cre* mice[42] were obtained
494 from The Jackson Laboratory (JAX stock #004781). These two mouse lines were
495 crossed to obtain macrophage-specific Adrb2 KO (MΦ-Adrb2KO) mice. All
496 experiments were performed with male mice at 10 weeks of age unless indicated
497 otherwise. Mice were anesthetized by intraperitoneal injection of a mixture of
498 medetomidine (0.3 mg/kg), midazolam (4.0 mg/kg), and butorphanol (5.0 mg/kg) and
499 were then subjected either to bilateral cast-immobilization of hind limbs with the use of
500 plastic tubes, adhesive tape, and animal bandage, or to bilateral hind limb denervation
501 by transection of the sciatic nerve. The immobilized mice were able to move freely
502 around their cages and to obtain food and water using their forelimbs. Animals were
503 analyzed 3 or 10 days after cast-immobilization or denervation unless indicated
504 otherwise. Mice were injected intraperitoneally with neutralizing antibodies to CXCL10
505 (MAB466, clone 134013; R&D Systems) or control IgG at 0.1 mg/body 3 days before
506 cast-immobilization, or with α-MT (Sigma-Aldrich) at 100 mg/kg, phentolamine
507 (Tokyo Chemical Industry) at 20 mg/kg, or propranolol (Sigma-Aldrich) at 10 mg/kg
508 daily for 10 days concomitant with cast-immobilization, or clenbuterol (Sigma-Aldrich)
509 at 1 mg/kg daily for 10 days. For fecal microbiota transplantation,[43] mice were
510 subjected to oral gavage with 200 µl supernatant of freshly collected fecal samples (50
511 mg/ml) or vehicle daily for 10 days. For antibiotic treatment, mice were subjected to
512 oral gavage with a cocktail of ampicillin (5 mg/ml), gentamicin (5 mg/ml), neomycin (5
513 mg/ml), metronidazole (5 mg/ml), and vancomycin (2.5 mg/ml) daily from 4 days
514 before immobilization, with or without cast-immobilization for 10 days. To deplete
515 macrophages in the colon,[44] mice were subjected to intrarectal injection of empty
516 liposome or clodronate liposome (Encapsula NanoSciences) at 500 µg/100 µl with
517 flexible catheter every other day from 4 days before immobilization, with or without
518 cast-immobilization for 10 days. Diets containing LA, HYD, or HYA (each at 1%) were
519 obtained from Noster and were administered to mice beginning 10 days before
520 immobilization. For chemical sympathectomy,[45] mice were subjected to intraperitoneal
521 injection of 6-OHDA (Sigma-Aldrich) at 80 mg/kg or vehicle (0.2% ascorbic acid,
522 Tocris Bioscience) daily for 3 days, with or without cast-immobilization for 10 days
523 starting 5 days after the final injection. *Cartpt-Cre* mice were described previously.[21]
524 AAV8-*hSyn-DIO-hM3D(Gq)-mCherry* was injected into the lower thoracic spinal cord,
525 and three weeks later, 2 mg/kg clozapine-N-oxide (CNO) or saline was administered
526 intraperitoneally daily for 7 days. The separation of blood cells from non–blood cells of

527 skeletal muscle was performed with the use of biotin-conjugated antibodies to mouse
528 CD45.2 (109804, BioLegend), microbeads conjugated with antibodies to biotin (130-
529 090-485, Miltenyi Biotec), and an autoMACS Pro Separator (Miltenyi Biotec). The
530 concentration of LPS or CXCL10 in the plasma or muscle tissue was measured using
531 the LAL endotoxin assay kit (GenScript) or the mouse CXCL10 DuoSet ELISA kit
532 (R&D Systems).
533
534 **Cell culture, RT-qPCR analysis, and immunoblot analysis**
535 C2C12 myoblasts were maintained and induced to differentiate into myotubes as
536 described previously,[46] and they were treated with LPS (L3129, Sigma-Aldrich) at 1
537 μg/ml for 6 h. Isolation of total RNA from cultured myotubes or from mouse or human
538 tissues as well as RT-qPCR analysis were performed as previously described,[46] and the
539 abundance of target mRNAs was normalized by that of 36B4 mRNA. The sequences of
540 mouse and human PCR primers are provided in Tables S2 and S3, respectively.
541 Immunoblot analysis was performed with antibodies to claudin-1 (2H10D10,
542 Invitrogen), GAPDH (M171-7, MBL), ERK (9102, Cell Signaling Technology), and
543 Thr^{202}/Tyr^{204}-phosphorylated ERK (9101, Cell Signaling Technology). Uncropped
544 immunoblots are shown in Figure S20.
545
546 **Histology and immunohistochemical staining**
547 Skeletal muscle or colon tissue sections were stained with hematoxylin-eosin or
548 subjected to immunohistochemical staining with antibodies to F4/80, myosin heavy
549 chain 7 (slow-twitch), or myosin heavy chain 1 (fast-twitch). Images were acquired with
550 a BZ-X710 fluorescence microscope (Keyence). The area of muscle fibers, depth of
551 crypts, and F4/80-positive area were quantified for each image with the use of ImageJ
552 software (NIH).
553
554 **Flow cytometry**
555 Skeletal muscle or the colon was minced and digested with 0.2% collagenase type II
556 (Worthington), the digested tissue was passed through 100-μm and 40-μm cell strainers
557 (Falcon), and erythrocytes were eliminated from the filtrate. The remaining cells were
558 exposed to antibodies to mouse CD16/32 (clone 93, 101302; BioLegend) before
559 staining with antibodies to the following proteins: CD45.2 (clone 104, 109822;
560 BioLegend), Ly6G (clone 1A8, 127606; BioLegend), F4/80 (clone BM8, 123116;
561 BioLegend), CD11b (clone M1/70, 101224; BioLegend), CD11c (clone N418, 117308;
562 BioLegend), and CD206 (clone C068C2, 141720; BioLegend). Dead cells were

excluded by staining with propidium iodide (421301, BioLegend). Events were acquired with an LSR Fortessa X-20 instrument (BD Biosciences) and analyzed with FlowJo software (BD Biosciences).

DNA microarray analysis

Total RNA extracted from gastrocnemius muscle of mice at 3 days after cast immobilization or of corresponding control animals was subjected to hybridization with an Affymetrix Mouse Gene 2.0 ST Array.

RNA-seq and scRNA-seq analysis

Total RNA extracted from gastrocnemius muscle, flexor carpi ulnaris, or colon tissue was subjected to RNA-seq analysis by Macrogen or Novogene. A paired-end library was prepared from each RNA sample with the use of a TruSeq Stranded mRNA Library Preparation Kit and was sequenced with a NovaSeq 6000 system (Illumina). Data were analyzed with RaNA-Seq[47] and DAVID Bioinformatics Resources 6.8. A Chromium Next GEM Single Cell Fixed RNA Sample Preparation Kit was used to isolate cells from colon tissue, and an scRNA-seq library was generated with a 10x Chromium system. Data analysis was performed by Genble.

Gut microbiota and metabolome analysis

DNA was extracted from feces with the use of a QIAamp PowerFecal Pro DNA Kit (Qiagen). For analysis of 16S rRNA genes of the gut microbiota, the V3-V4 region of the gene was amplified from the extracted DNA with 341F (5′-TCGTCGGCAGCGTCAGATGTGTATAAGCGACAGCCTACGGGNGGCWGCAG-3′) and 805R (5′-GTCTCGTGGGCTCGGAGATGTGTATAAGAGACAGGACTACHVGGGTATCTAATCC-3′) primers. Both ends of the amplified fragments were tagged with the use of a Nextera XT Index Kit v2 (Illumina), and the amplicons were then purified and sequenced with the use of an Illumina MiSeq system and MiSeq Reagent Kit v3. Postsequencing analysis was performed with the Quantitative Insights Into Microbial Ecology 2 (QIIME2) pipeline. SILVA (version SSU138.1) was adopted as a reference sequence database for estimation of bacterial species prevalence, and gut microbiota composition was determined with OTUs, which grouped reads with a sequence identity of ≥97%. Comprehensive analysis of gut microbial lipid metabolites was performed as previously described.[48]

599 **Measurement of NE turnover**
600 NE turnover was measured on the basis of the decline in tissue NE content after
601 inhibition of catecholamine biosynthesis with α-MT as described previously.[19,20] Mice
602 were injected intraperitoneally with α-MT at 300 mg/kg. At 0 or 4 h after α-MT
603 injection, the animals were decapitated and tissues were rapidly removed and weighed.
604 Tissue samples were homogenized in 0.2 M perchloric acid containing 0.1 mM EDTA,
605 the homogenate was centrifuged at 4°C, and NE or DHPG was purified from the
606 resulting supernatant with activated alumina and measured by high-performance liquid
607 chromatography with electrochemical detection. Data are expressed as picograms of NE
608 or DHPG per milligram of tissue weight.
609
610 **Human skeletal muscle samples**
611 Specimens of human skeletal muscle were obtained as previously described.[6] In brief,
612 samples were obtained from 15 individuals at an average of 8.3 ± 3.1 days after fixation
613 surgery for a bone fracture of the arm or leg as well as from 18 control participants who
614 underwent implant-removal surgery 6 to 12 months after fixation surgery.
615
616 **Publicly available human gene expression data analysis**
617 For the analysis of publicly available human gene expression data, the process of data
618 set selection was undertaken as follows. NCBI GEO and Array Express databases were
619 searched with the terms "muscle", "cast", "immobilization", and "human". Screening of
620 the three identified data sets resulted in the exclusion of one (GSE45462) because it
621 included only individuals with fractures. The remaining two data sets (GSE14901 and
622 GSE8872) underwent eligibility assessment, with GSE8872 being subsequently
623 excluded on the basis of a small number of healthy subjects (n = 2). The remaining data
624 set (GSE14901) met all the inclusion criteria and was adopted for analysis.
625
626 **Statistical analysis**
627 Quantitative data were presented as means ± SEM or as medians with the interquartile
628 range, and they were analyzed by the two-tailed unpaired Student's t test, two-way
629 analysis of variance (ANOVA) with Bonferroni's post hoc test, the Mann-Whitney U
630 test, or one-way ANOVA followed by Dunnett's test or Bonferroni's post hoc test. A p
631 value of <0.05 was considered statistically significant. All statistical analysis was
632 performed with the use of GraphPad Prism 9 (GraphPad Software).
633
634 **Study approval**

635 All animal experiments were approved by the animal experimentation committee of
636 Kobe University Graduate School of Medicine (approval no. P221201). Human
637 experiments were approved by the medical ethics committee of Kobe University
638 Graduate School of Medicine (approval no. 180059), and all subjects provided written
639 informed consent.
640
641 **Data availability**
642 The microarray data have been deposited in NCBI Gene Expression Omnibus (GEO)
643 under the accession number GSE172501. The RNA-seq data have been deposited in
644 NCBI GEO under the accession numbers GSE249515 (mouse gastrocnemius),
645 GSE288180 (mouse flexor carpi ulnaris), and GSE249324 (mouse colon). The scRNA-
646 seq data have been deposited in NCBI GEO under the accession number GSE265821.
647

References

1. Kalyani, R.R., Corriere, M. & Ferrucci, L. Age-related and disease-related muscle loss: the effect of diabetes, obesity, and other diseases. *Lancet Diabetes Endocrinol* **2**, 819-829 (2014).
2. Cartee, G.D., Hepple, R.T., Bamman, M.M. & Zierath, J.R. Exercise Promotes Healthy Aging of Skeletal Muscle. *Cell Metab.* **23**, 1034-1047 (2016).
3. Preobrazenski, N., Seigel, J., Halliday, S., Janssen, I. & McGlory, C. Single-leg disuse decreases skeletal muscle strength, size, and power in uninjured adults: A systematic review and meta-analysis. *J Cachexia Sarcopenia Muscle* **14**, 684-696 (2023).
4. Gao, Y., Arfat, Y., Wang, H. & Goswami, N. Muscle Atrophy Induced by Mechanical Unloading: Mechanisms and Potential Countermeasures. *Front. Physiol.* **9**, 235 (2018).
5. Hardy, E.J.O.*, et al.* The time course of disuse muscle atrophy of the lower limb in health and disease. *J Cachexia Sarcopenia Muscle* **13**, 2616-2629 (2022).
6. Hirata, Y.*, et al.* A Piezo1/KLF15/IL-6 axis mediates immobilization-induced muscle atrophy. *J. Clin. Invest.* **132**, 1-13 (2022).
7. Saitou, K.*, et al.* Local cyclical compression modulates macrophage function in situ and alleviates immobilization-induced muscle atrophy. *Clin. Sci. (Lond.)* **132**, 2147-2161 (2018).
8. Kawanishi, N., Funakoshi, T. & Machida, S. Time-course study of macrophage infiltration and inflammation in cast immobilization-induced atrophied muscle of mice. *Muscle Nerve* **57**, 1006-1013 (2018).
9. Hoff, P.*, et al.* Effects of 60-day bed rest with and without exercise on cellular and humoral immunological parameters. *Cell. Mol. Immunol.* **12**, 483-492 (2015).
10. Berchiche, Y.A. & Sakmar, T.P. CXC Chemokine Receptor 3 Alternative Splice Variants Selectively Activate Different Signaling Pathways. *Mol. Pharmacol.* **90**, 483-495 (2016).
11. Kawano, Y.*, et al.* Colonic Pro-inflammatory Macrophages Cause Insulin Resistance in an Intestinal Ccl2/Ccr2-Dependent Manner. *Cell Metab.* **24**, 295-310 (2016).
12. Tilg, H., Zmora, N., Adolph, T.E. & Elinav, E. The intestinal microbiota fuelling metabolic inflammation. *Nat. Rev. Immunol.* **20**, 40-54 (2020).
13. Garcia-Hernandez, V., Quiros, M. & Nusrat, A. Intestinal epithelial claudins: expression and regulation in homeostasis and inflammation. *Ann. N. Y. Acad. Sci.* **1397**, 66-79 (2017).
14. Kishino, S.*, et al.* Polyunsaturated fatty acid saturation by gut lactic acid bacteria

684 affecting host lipid composition. *Proc. Natl. Acad. Sci. U. S. A.* **110**, 17808-17813
685 (2013).
686 15. Miyamoto, J.*, et al.* A gut microbial metabolite of linoleic acid, 10-hydroxy-cis-12-
687 octadecenoic acid, ameliorates intestinal epithelial barrier impairment partially via
688 GPR40-MEK-ERK pathway. *J. Biol. Chem.* **290**, 2902-2918 (2015).
689 16. Hirata, A.*, et al.* A novel unsaturated fatty acid hydratase toward C16 to C22 fatty
690 acids from Lactobacillus acidophilus. *J. Lipid Res.* **56**, 1340-1350 (2015).
691 17. Yang, D., Almanzar, N. & Chiu, I.M. The role of cellular and molecular
692 neuroimmune crosstalk in gut immunity. *Cell. Mol. Immunol.* **20**, 1259-1269 (2023).
693 18. Populin, L., Stebbing, M.J. & Furness, J.B. Neuronal regulation of the gut immune
694 system and neuromodulation for treating inflammatory bowel disease. *FASEB*
695 *Bioadv* **3**, 953-966 (2021).
696 19. Saito, M., Minokoshi, Y. & Shimazu, T. Accelerated norepinephrine turnover in
697 peripheral tissues after ventromedial hypothalamic stimulation in rats. *Brain Res.*
698 **481**, 298-303 (1989).
699 20. Shiuchi, T.*, et al.* Hypothalamic orexin stimulates feeding-associated glucose
700 utilization in skeletal muscle via sympathetic nervous system. *Cell Metab.* **10**, 466-
701 480 (2009).
702 21. Harima, Y.*, et al.* Parallel labeled-line organization of sympathetic outflow for
703 selective organ regulation in mice. *Nat Commun* **15**, 10478 (2024).
704 22. Kuramoto, N.*, et al.* Role of PDK1 in skeletal muscle hypertrophy induced by
705 mechanical load. *Sci. Rep.* **11**, 3447 (2021).
706 23. Lynch, G.S. & Ryall, J.G. Role of beta-adrenoceptor signaling in skeletal muscle:
707 implications for muscle wasting and disease. *Physiol. Rev.* **88**, 729-767 (2008).
708 24. Wang, X., Yu, L. & Wu, A.R. The effect of methanol fixation on single-cell RNA
709 sequencing data. *BMC Genomics* **22**, 420 (2021).
710 25. van Eijck, C.W.F.*, et al.* Enhanced antitumour immunity following neoadjuvant
711 chemoradiotherapy mediates a favourable prognosis in women with resected
712 pancreatic cancer. *Gut* **73**, 311-324 (2024).
713 26. Armet, A.M.*, et al.* Rethinking healthy eating in light of the gut microbiome. *Cell*
714 *Host Microbe* **30**, 764-785 (2022).
715 27. Brown, E.M., Clardy, J. & Xavier, R.J. Gut microbiome lipid metabolism and its
716 impact on host physiology. *Cell Host Microbe* **31**, 173-186 (2023).
717 28. Miyamoto, J.*, et al.* Gut microbiota confers host resistance to obesity by
718 metabolizing dietary polyunsaturated fatty acids. *Nat Commun* **10**, 4007 (2019).
719 29. Kaikiri, H.*, et al.* Supplemental feeding of a gut microbial metabolite of linoleic

720 acid, 10-hydroxy-cis-12-octadecenoic acid, alleviates spontaneous atopic dermatitis
721 and modulates intestinal microbiota in NC/nga mice. *Int. J. Food Sci. Nutr.* **68**, 941-
722 951 (2017).
723 30. Kasahara, N.*, et al.* A gut microbial metabolite of linoleic acid ameliorates liver
724 fibrosis by inhibiting TGF-beta signaling in hepatic stellate cells. *Sci. Rep.* **13**,
725 18983 (2023).
726 31. Yamada, M.*, et al.* A bacterial metabolite ameliorates periodontal pathogen-induced
727 gingival epithelial barrier disruption via GPR40 signaling. *Sci. Rep.* **8**, 9008 (2018).
728 32. Moriyama, S.*, et al.* beta(2)-adrenergic receptor-mediated negative regulation of
729 group 2 innate lymphoid cell responses. *Science* **359**, 1056-1061 (2018).
730 33. Wang, P.*, et al.* Adrenergic nerves regulate intestinal regeneration through IL-22
731 signaling from type 3 innate lymphoid cells. *Cell Stem Cell* **30**, 1166-1178 e1168
732 (2023).
733 34. Gabanyi, I.*, et al.* Neuro-immune Interactions Drive Tissue Programming in
734 Intestinal Macrophages. *Cell* **164**, 378-391 (2016).
735 35. Matheis, F.*, et al.* Adrenergic Signaling in Muscularis Macrophages Limits
736 Infection-Induced Neuronal Loss. *Cell* **180**, 64-78 e16 (2020).
737 36. Galzi, J.L.*, et al.* Neutralizing endogenous chemokines with small molecules.
738 Principles and potential therapeutic applications. *Pharmacol. Ther.* **126**, 39-55
739 (2010).
740 37. van den Borne, P., Quax, P.H., Hoefer, I.E. & Pasterkamp, G. The multifaceted
741 functions of CXCL10 in cardiovascular disease. *Biomed Res Int* **2014**, 893106
742 (2014).
743 38. Sasaki, Y.*, et al.* Blockade of the CXCR3/CXCL10 axis ameliorates inflammation
744 caused by immunoproteasome dysfunction. *JCI Insight* **7**(2022).
745 39. Yellin, M.*, et al.* A phase II, randomized, double-blind, placebo-controlled study
746 evaluating the efficacy and safety of MDX-1100, a fully human anti-CXCL10
747 monoclonal antibody, in combination with methotrexate in patients with
748 rheumatoid arthritis. *Arthritis Rheum.* **64**, 1730-1739 (2012).
749 40. Alex Klarenbeek, D.M., Christophe Blanchetot, Michael Saunders, Sebastian van
750 der Woning, Martine Smit, Hans de Haard, Erik Hofman. Targeting chemokines
751 and chemokine receptors with antibodies. *Drug Discov Today Technol* **9**, e227-314
752 (2012).
753 41. Hinoi, E.*, et al.* The sympathetic tone mediates leptin's inhibition of insulin
754 secretion by modulating osteocalcin bioactivity. *J. Cell Biol.* **183**, 1235-1242 (2008).
755 42. Clausen, B.E., Burkhardt, C., Reith, W., Renkawitz, R. & Forster, I. Conditional

gene targeting in macrophages and granulocytes using LysMcre mice. *Transgenic Res.* **8**, 265-277 (1999).

43. Wouters, S.*, et al.* Protocol for fecal microbiota transplantation: A microaerophilic approach for mice housed in a specific pathogen-free facility. *STAR Protoc* **6**, 103517 (2025).

44. Rohm, T.V.*, et al.* Targeting colonic macrophages improves glycemic control in high-fat diet-induced obesity. *Commun Biol* **5**, 370 (2022).

45. Tyus, D.*, et al.* The sympathetic nervous system drives hyperinflammatory responses to Clostridioides difficile infection. *Cell Rep Med* **5**, 101771 (2024).

46. Hirata, Y.*, et al.* Hyperglycemia induces skeletal muscle atrophy via a WWP1/KLF15 axis. *JCI Insight* **4**(2019).

47. Prieto, C. & Barrios, D. RaNA-Seq: Interactive RNA-Seq analysis from FASTQ files to functional analysis. *Bioinformatics* (2019).

48. Tsuji, K., Shimada, W., Kishino, S., Ogawa, J. & Arita, M. Comprehensive analysis of fatty acid metabolites produced by gut microbiota using LC-MS/MS-based lipidomics. *Medical Mass Spectrometry* **6**, 112-125 (2022).

Figure 1

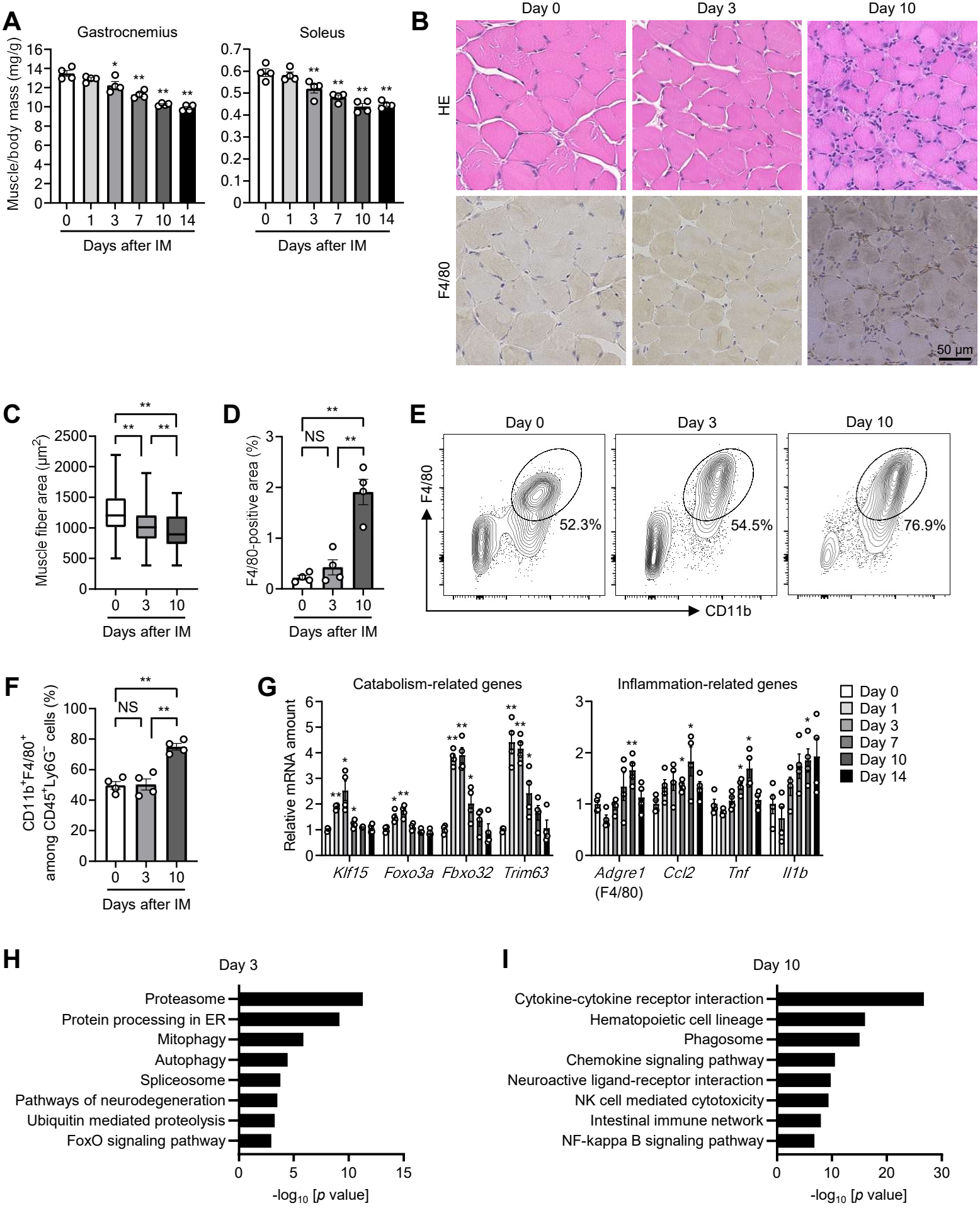
A
Gastrocnemius
Soleus
Muscle/body mass (mg/g)
Days after IM
B
Day 0
Day 3
Day 10
HE
F4/80
50 μm
C
Muscle fiber area (μm²)
Days after IM
D
F4/80-positive area (%)
NS
Days after IM
E
Day 0
Day 3
Day 10
F4/80
CD11b
52.3%
54.5%
76.9%
F
CD11b⁺F4/80⁺ among CD45⁺Ly6G⁻ cells (%)
NS
Days after IM
G
Catabolism-related genes
Inflammation-related genes
Relative mRNA amount
Klf15
Foxo3a
Fbxo32
Trim63
Adgre1 (F4/80)
Ccl2
Tnf
Il1b
Day 0
Day 1
Day 3
Day 7
Day 10
Day 14
H
Day 3
Proteasome
Protein processing in ER
Mitophagy
Autophagy
Spliceosome
Pathways of neurodegeneration
Ubiquitin mediated proteolysis
FoxO signaling pathway
-log10 [p value]
I
Day 10
Cytokine-cytokine receptor interaction
Hematopoietic cell lineage
Phagosome
Chemokine signaling pathway
Neuroactive ligand-receptor interaction
NK cell mediated cytotoxicity
Intestinal immune network
NF-kappa B signaling pathway
-log10 [p value]

Figure 1. Transition from protein catabolism to inflammation during skeletal muscle immobilization

(A) Ratio of gastrocnemius and soleus muscle mass for both hind limbs to body mass for mice subjected to bilateral hind limb immobilization (IM) by cast-fixation for the indicated times (n = 4 mice).

(B–D) Hematoxylin-eosin (HE) staining and immunohistochemical staining of F4/80 (B) for determination of muscle fiber area (C) and the F4/80-positive area (D) in soleus muscle of mice subjected to hind limb immobilization for the indicated times (n = 4 mice). The area of 800 fibers pooled from four mice was measured and averaged for each condition in (C). Scale bar (B), 50 μm.

(E and F) Representative flow cytometric analysis (E) and the percentage (F) of $CD11b^{+}F4/80^{+}$ cells among $CD45^{+}Ly6G^{-}$ cells in immobilized skeletal muscle (n = 4 mice).

(G) RT-qPCR analysis of protein catabolism– or inflammation-related gene expression in gastrocnemius muscle of immobilized mice (n = 4 mice).

(H and I) Kyoto Encyclopedia of Genes and Genomes (KEGG) pathway analysis for RNA-seq data from the gastrocnemius at 3 days (H) or 10 days (I) after hind limb immobilization. The top eight pathways enriched among genes whose expression was upregulated by immobilization are shown.

Quantitative data are presented as means ± SEM (A, D, F, and G) or medians with interquartile range (C). *$p < 0.05$, **$p < 0.01$, NS (not significant) compared with day 0 (A and G) or as indicated (C, D, and F) by two-way ANOVA with the Bonferroni post hoc test.

Figure 2

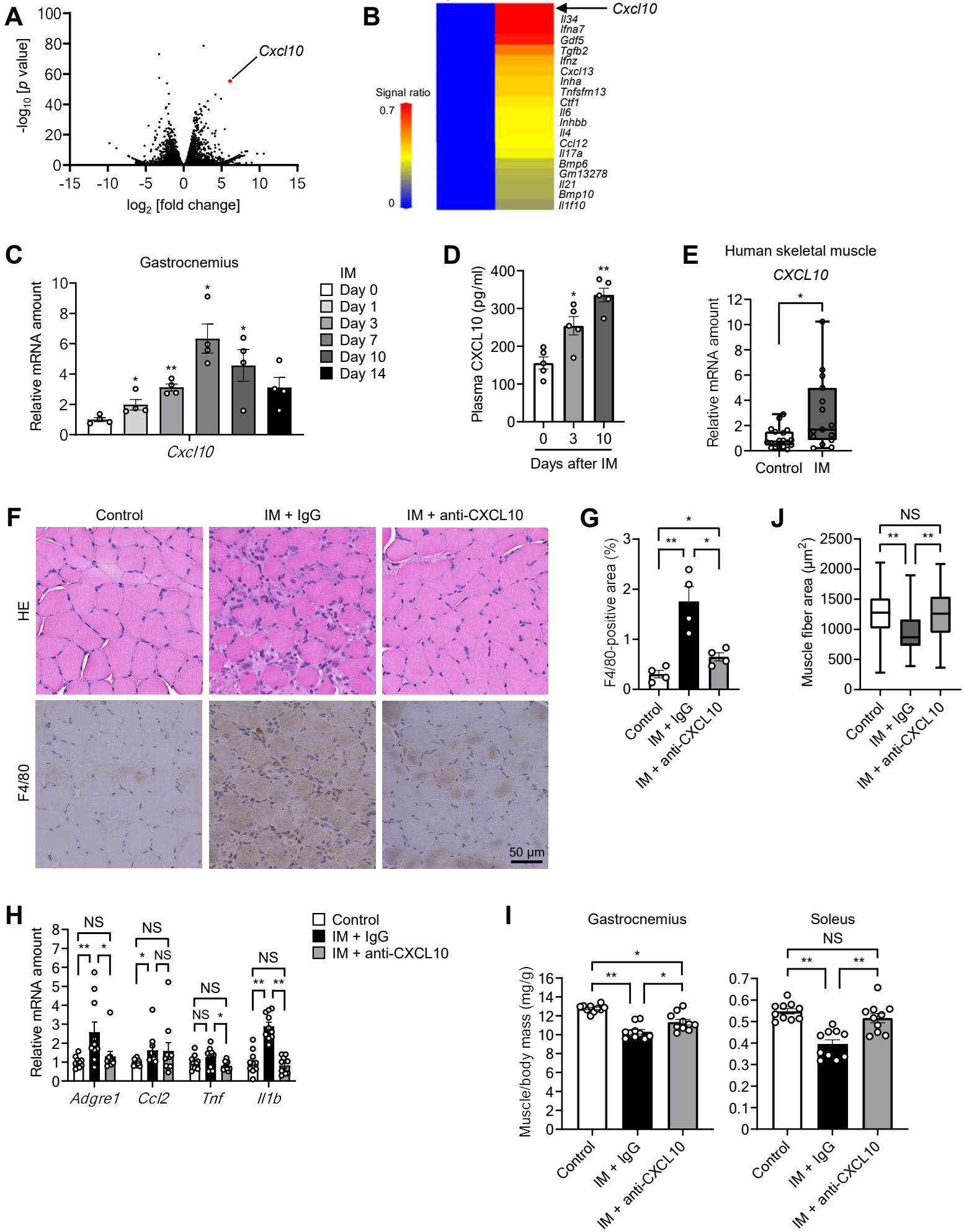
A
-log10 [p value]
log2 [fold change]
Cxcl10
B
Control
IM
Cxcl10
Il34
Ifna7
Gdf5
Tgfb2
Ifnz
Cxcl13
Inha
Tnfsfm13
Ctf1
Il6
Inhbb
Il4
Ccl12
Il17a
Bmp6
Gm13278
Il21
Bmp10
Il1f10
Signal ratio
0.7
0
C
Gastrocnemius
Relative mRNA amount
Cxcl10
IM
Day 0
Day 1
Day 3
Day 7
Day 10
Day 14
D
Plasma CXCL10 (pg/ml)
Days after IM
E
Human skeletal muscle
CXCL10
Relative mRNA amount
Control
IM
F
Control
IM + IgG
IM + anti-CXCL10
HE
F4/80
50 μm
G
F4/80-positive area (%)
Control
IM + IgG
IM + anti-CXCL10
J
NS
Muscle fiber area (μm2)
Control
IM + IgG
IM + anti-CXCL10
H
Relative mRNA amount
NS
Adgre1
Ccl2
Tnf
Il1b
Control
IM + IgG
IM + anti-CXCL10
I
Gastrocnemius
Soleus
Muscle/body mass (mg/g)
Control
IM + IgG
IM + anti-CXCL10

Figure 2. CXCL10 mediates inflammation and atrophy of muscle induced by limb immobilization

(A and B) Volcano plot of RNA-seq data (A) and heat map of inflammation-related gene expression determined by DNA microarray analysis (B) for gastrocnemius of mice subjected to cast-immobilization for 3 days compared with control mice.

(C) RT-qPCR analysis of *Cxcl10* mRNA abundance in gastrocnemius of cast-immobilized mice (n = 4 mice).

(D) Plasma concentration of CXCL10 in cast-immobilized mice (n = 5 mice).

(E) RT-qPCR analysis of *CXCL10* mRNA in skeletal muscle of human individuals subjected to cast-fixation (n = 15) or of control subjects (n = 18).

(F–J) Hematoxylin-eosin and F4/80 immunohistochemical staining (F) and the F4/80-positive area (G) of soleus (n = 4 mice), RT-qPCR analysis of inflammation-related gene expression in gastrocnemius (n = 10 mice) (H), the ratio of muscle mass to body mass (n = 10 mice) (I), and muscle fiber area in soleus (n = 4 mice) (J) for control mice or mice subjected to intraperitoneal injection of neutralizing antibodies to CXCL10 (0.1 mg/body) or control immunoglobulin G (IgG) 3 days before cast-immobilization for 10 days. Scale bar (F), 50 μm. The area of 800 fibers pooled from four mice was measured and averaged for each condition in (J).

Quantitative data are presented as means ± SEM (C, D, G, H, and I) or medians with interquartile range (E and J). *$p < 0.05$, **$p < 0.01$, NS relative to day 0 (C and D) or as indicated (E and G–J) by the Mann-Whitney U test (E) or two-way ANOVA with the Bonferroni post hoc test (C, D, and G–J).

Figure 3

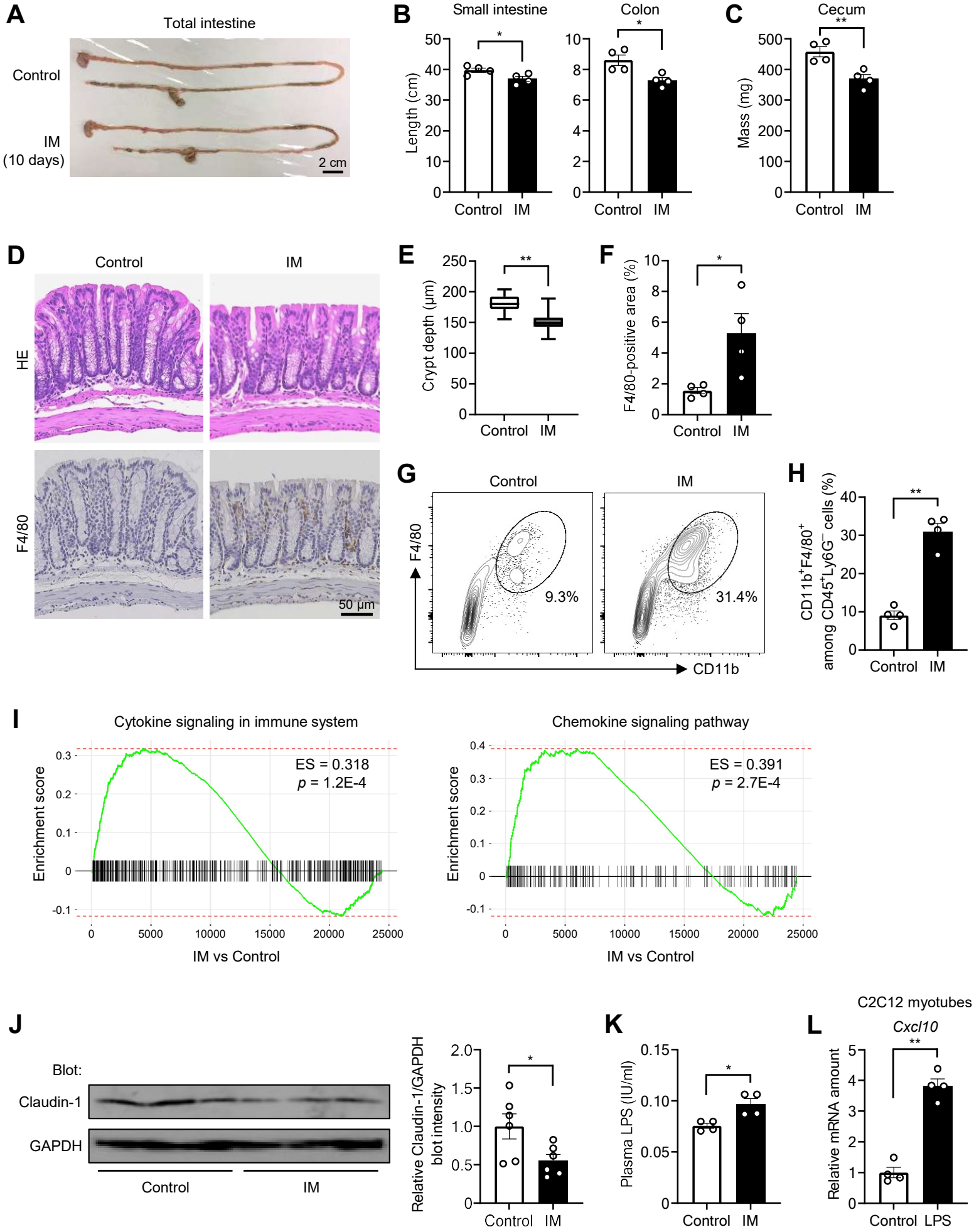
A
Total intestine
Control
IM
(10 days)
2 cm
B
Small intestine
Colon
Length (cm)
Control
IM
C
Cecum
Mass (mg)
D
Control
IM
HE
F4/80
50 μm
E
Crypt depth (μm)
F
F4/80-positive area (%)
G
F4/80
CD11b
9.3%
31.4%
H
CD11b+F4/80+ among CD45+Ly6G− cells (%)
I
Cytokine signaling in immune system
ES = 0.318
p = 1.2E-4
Enrichment score
IM vs Control
Chemokine signaling pathway
ES = 0.391
p = 2.7E-4
J
Blot:
Claudin-1
GAPDH
Relative Claudin-1/GAPDH blot intensity
K
Plasma LPS (IU/ml)
L
C2C12 myotubes
Cxcl10
Relative mRNA amount
LPS

Figure 3. Prolonged limb immobilization induces inflammation in the intestine
(A–F) Representative images of the entire intestine (A), length of the small intestine and colon (B), mass of the cecum (C), and hematoxylin-eosin and F4/80 immunohistochemical staining (D) for determination of crypt depth (E) and the F4/80-positive area (F) in the colon of control mice or mice subjected to cast-immobilization for 10 days (n = 4 mice). Scale bars, 2 cm (A) and 50 μm (D). The depth of 100 crypts pooled from four mice was measured and averaged for each condition in (E).
(G and H) Representative flow cytometric analysis (G) and the percentage (H) of $CD11b^{+}F4/80^{+}$ cells among $CD45^{+}Ly6G^{-}$ cells in the colon of immobilized and control mice (n = 4 mice).
(I) GSEA of RNA-seq data obtained from the colon of immobilized and control mice.
(J and K) Immunoblot analysis of claudin-1 and GAPDH (loading control) in the colon (n = 6 mice) (J) and the plasma concentration of LPS (n = 4 mice) (K) for mice subjected (or not) to cast-immobilization for 10 days.
(L) RT-qPCR analysis of *Cxcl10* mRNA abundance in C2C12 myotubes exposed to LPS (1 μg/ml) or vehicle (control) for 6 h (n = 4 independent experiments).
Quantitative data are presented as means ± SEM (B, C, F, H, and J–L) or medians with interquartile range (E). *$p < 0.05$, **$p < 0.01$ (unpaired Student's t test).

Figure 4

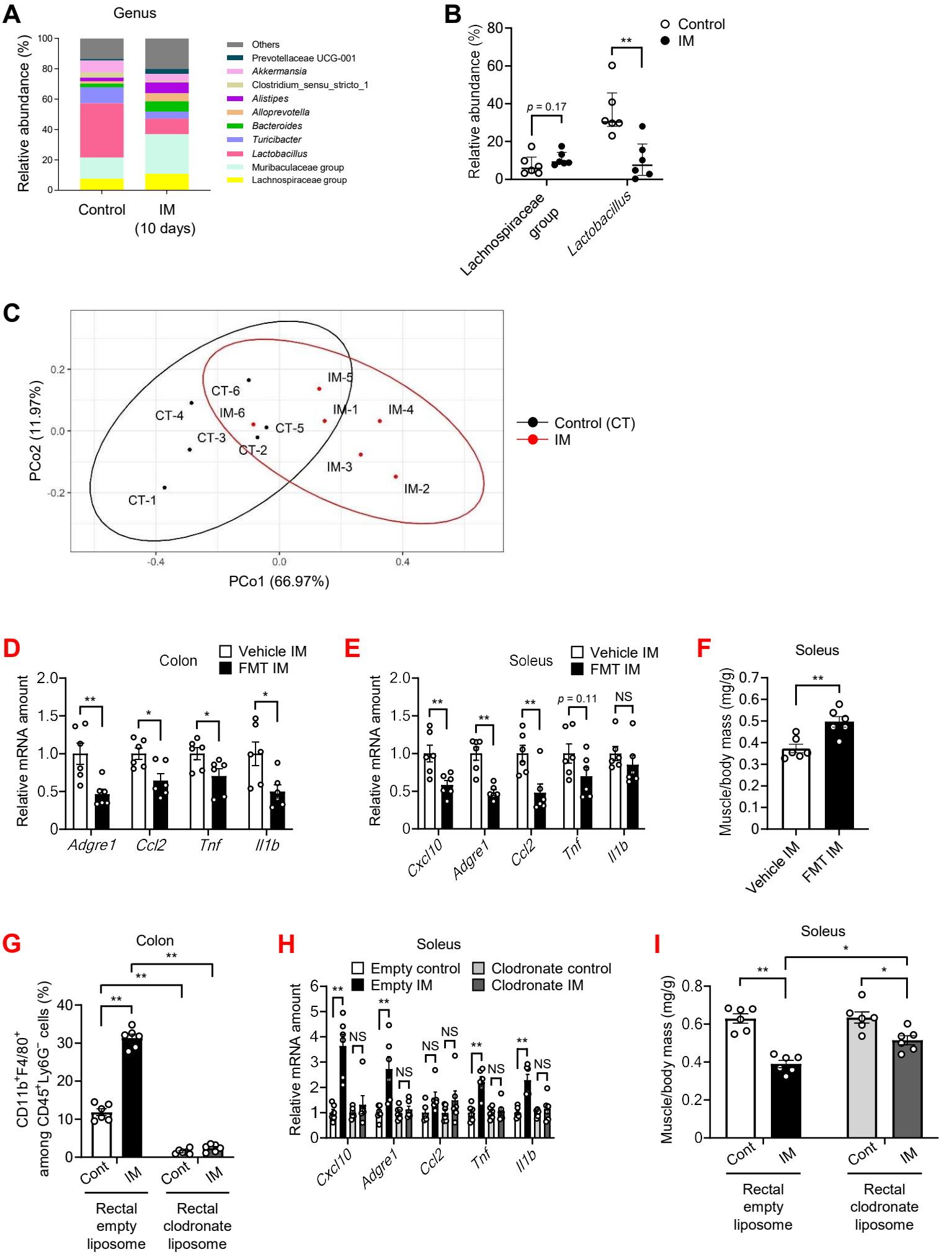
A
Genus
Relative abundance (%)
Control
IM
(10 days)
Others
Prevotellaceae UCG-001
Akkermansia
Clostridium_sensu_stricto_1
Alistipes
Alloprevotella
Bacteroides
Turicibacter
Lactobacillus
Muribaculaceae group
Lachnospiraceae group
B
Relative abundance (%)
Control
IM
p = 0.17
**
Lachnospiraceae group
Lactobacillus
C
PCo2 (11.97%)
PCo1 (66.97%)
CT-1
CT-2
CT-3
CT-4
CT-5
CT-6
IM-1
IM-2
IM-3
IM-4
IM-5
IM-6
Control (CT)
IM
D
Colon
Vehicle IM
FMT IM
Relative mRNA amount
Adgre1
Ccl2
Tnf
Il1b
E
Soleus
Vehicle IM
FMT IM
Relative mRNA amount
p = 0.11
NS
Cxcl10
Adgre1
Ccl2
Tnf
Il1b
F
Soleus
Muscle/body mass (mg/g)
Vehicle IM
FMT IM
G
Colon
CD11b+F4/80+ among CD45+Ly6G- cells (%)
Cont
IM
Rectal empty liposome
Rectal clodronate liposome
H
Soleus
Empty control
Empty IM
Clodronate control
Clodronate IM
Relative mRNA amount
NS
Cxcl10
Adgre1
Ccl2
Tnf
Il1b
I
Soleus
Muscle/body mass (mg/g)
Cont
IM
Rectal empty liposome
Rectal clodronate liposome

Figure 4. The gut microbiota and intestinal macrophages contribute to inflammation and atrophy of skeletal muscle induced by immobilization

(A–C) Gut microbial composition at the genus level determined by analysis of bacterial 16S rRNA genes (A), relative abundance of the Lachnospiraceae group and *Lactobacillus* species (B), and corresponding principal coordinate analysis (C) for control mice or mice subjected to cast-immobilization for 10 days (n = 6 mice).

(D–F) RT-qPCR analysis of inflammation-related gene expression in the colon (D) and soleus (E), and ratio of soleus muscle mass to body mass (F) of cast-immobilized mice subjected to fecal microbiota transplantation (FMT) or vehicle by oral gavage daily for 10 days (n = 6 mice).

(G–I) The percentage of $CD11b^{+}F4/80^{+}$ cells among $CD45^{+}Ly6G^{-}$ cells in the colon (G), RT-qPCR analysis of inflammation-related gene expression in soleus (H), and ratio of soleus muscle mass to body mass (I) of mice subjected to intrarectal injection of empty liposome or clodronate liposome every other day from 4 days before immobilization, with or without cast-immobilization for 10 days (n = 6 mice).

Quantitative data are presented as means ± SEM (D–I) or medians with interquartile range (B). *$p < 0.05$, **$p < 0.01$, NS by the Mann-Whitney U test (B), the unpaired Student's t test (D–F), or two-way ANOVA with the Bonferroni post hoc test (G–I).

Figure 5

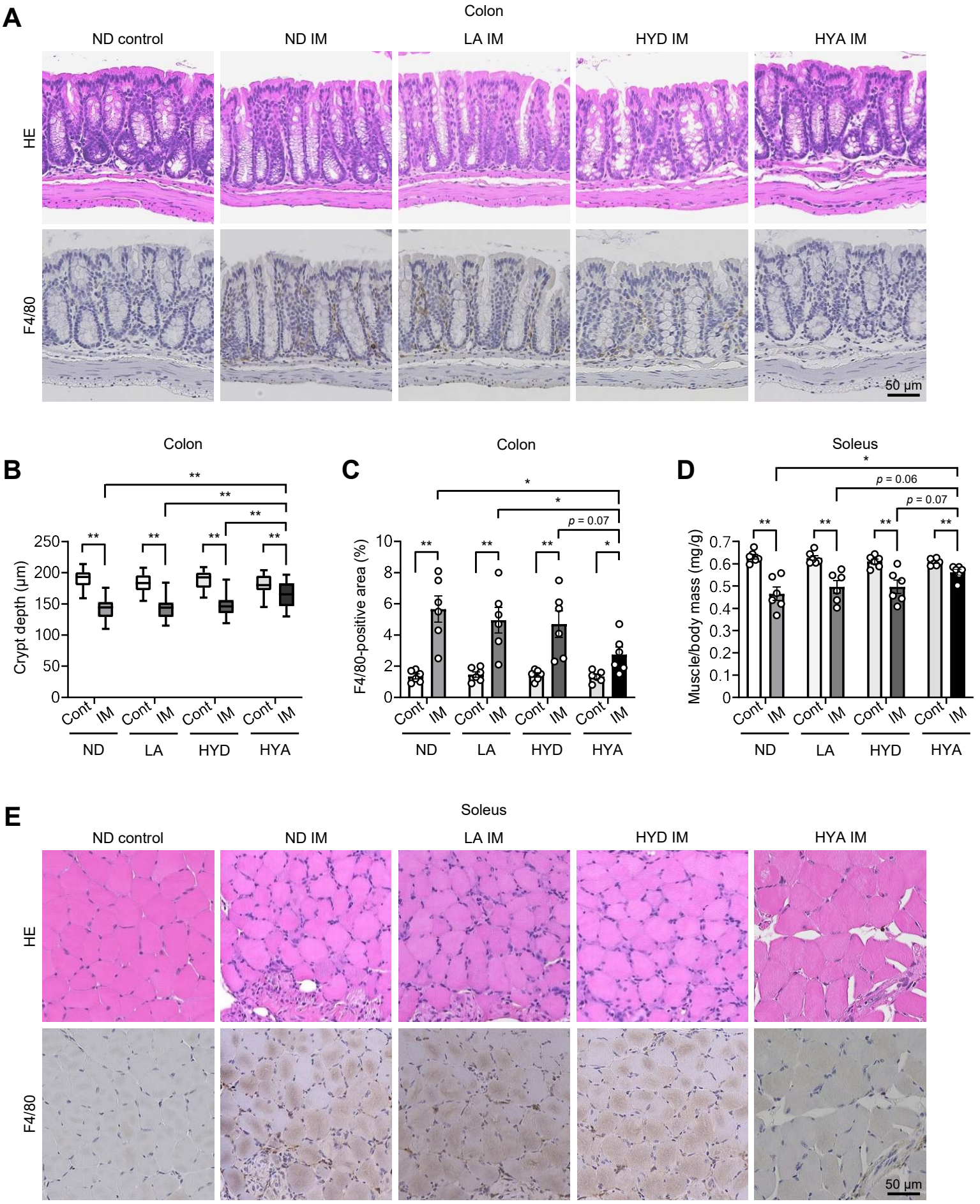
A
Colon
ND control
ND IM
LA IM
HYD IM
HYA IM
HE
F4/80
50 μm
B
Colon
Crypt depth (μm)
Cont
IM
ND
LA
HYD
HYA
C
Colon
F4/80-positive area (%)
p = 0.07
D
Soleus
Muscle/body mass (mg/g)
p = 0.06
p = 0.07
E
Soleus
ND control
ND IM
LA IM
HYD IM
HYA IM
HE
F4/80
50 μm

Figure 5. A gut microbial metabolite derived from LA inhibits intestinal and muscle inflammation as well as muscle atrophy induced by limb immobilization

(A–C) Hematoxylin-eosin and F4/80 immunohistochemical staining (A) for determination of crypt depth (B) and the F4/80-positive area (C) in the colon of mice fed a normal diet (ND) or a diet containing LA, HYD, or HYA and subjected (or not) to cast-fixation of the hind limbs for 10 days (n = 6 mice). The depth of 100 crypts pooled from four mice was measured and averaged for each condition in (B). Scale bar (A), 50 μm.

(D and E) Ratio of muscle mass to body mass (D) as well as hematoxylin-eosin and F4/80 immunohistochemical staining (E) for the soleus of mice (n = 6) treated as in (A) to (C). Scale bar (E), 50 μm.

Quantitative data are presented as means ± SEM (C and D) or medians with interquartile range (B). *$p < 0.05$, **$p < 0.01$ (two-way ANOVA with the Bonferroni post hoc test).

Figure 6

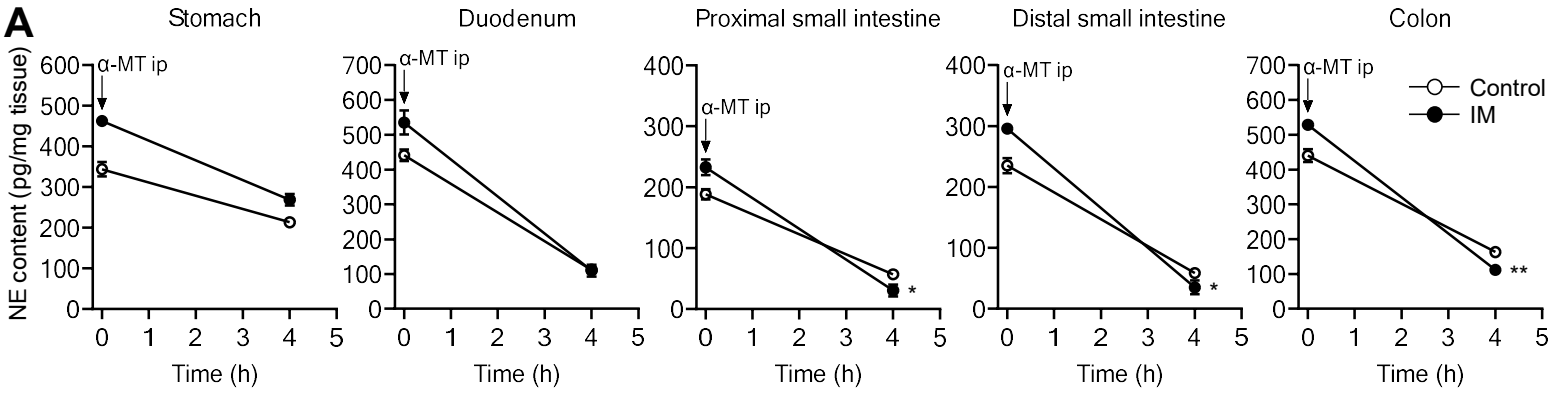
A
Stomach
Duodenum
Proximal small intestine
Distal small intestine
Colon
NE content (pg/mg tissue)
α-MT ip
Control
IM
Time (h)

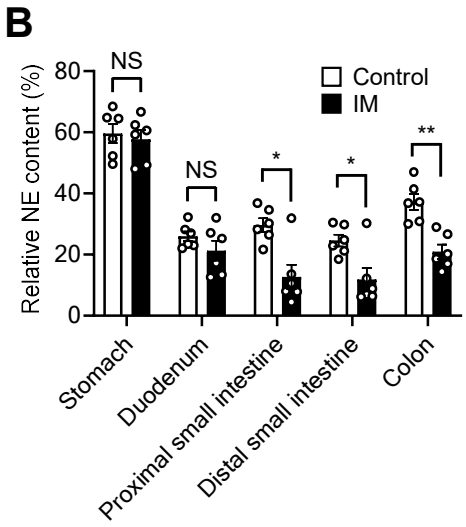
B
Relative NE content (%)
NS
Control
IM
Stomach
Duodenum
Proximal small intestine
Distal small intestine
Colon

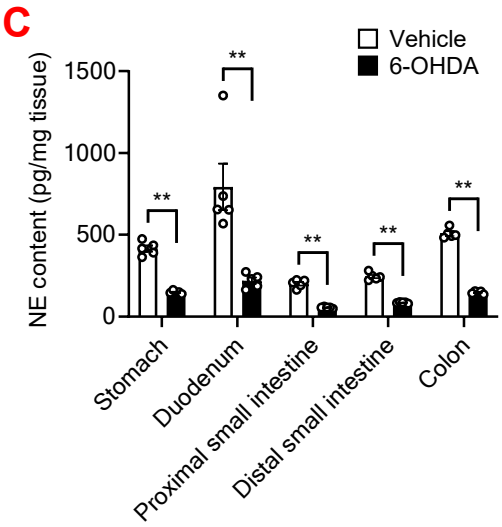
C
NE content (pg/mg tissue)
Vehicle
6-OHDA
Stomach
Duodenum
Proximal small intestine
Distal small intestine
Colon

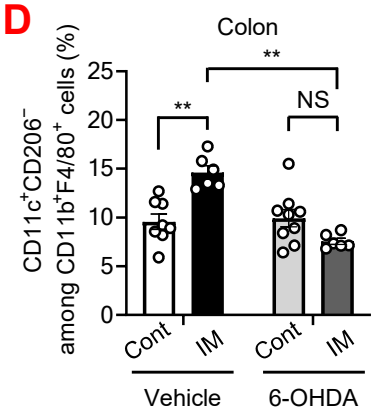
D
Colon
among CD11b+F4/80+ cells (%)
CD11c+CD206−
NS
Cont
IM
Vehicle
6-OHDA

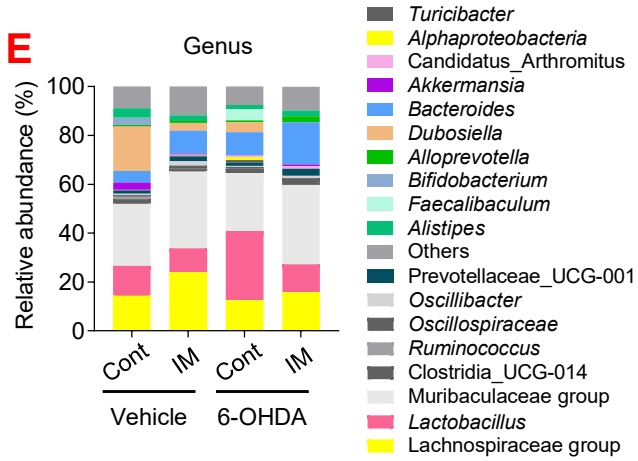
E
Genus
Relative abundance (%)
Cont
IM
Vehicle
6-OHDA
Turicibacter
Alphaproteobacteria
Candidatus_Arthromitus
Akkermansia
Bacteroides
Dubosiella
Alloprevotella
Bifidobacterium
Faecalibaculum
Alistipes
Others
Prevotellaceae_UCG-001
Oscillibacter
Oscillospiraceae
Ruminococcus
Clostridia_UCG-014
Muribaculaceae group
Lactobacillus
Lachnospiraceae group

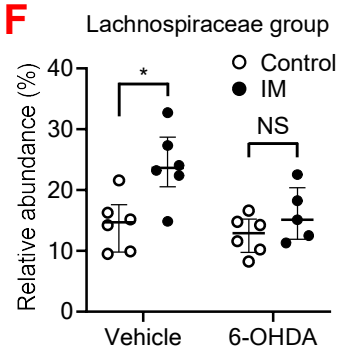
F
Lachnospiraceae group
Relative abundance (%)
Control
IM
NS
Vehicle
6-OHDA

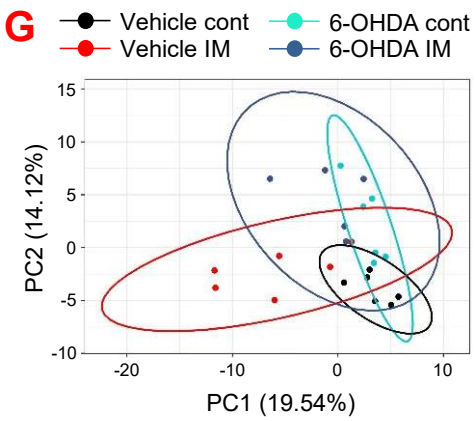
G
Vehicle cont
Vehicle IM
6-OHDA cont
6-OHDA IM
PC2 (14.12%)
PC1 (19.54%)

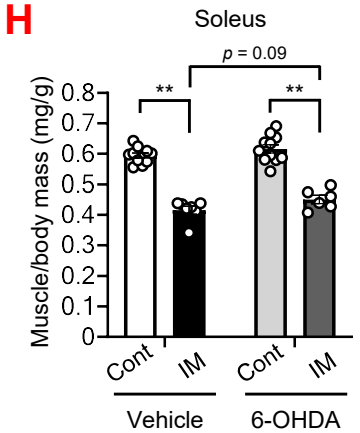
H
Soleus
p = 0.09
Muscle/body mass (mg/g)
Cont
IM
Vehicle
6-OHDA

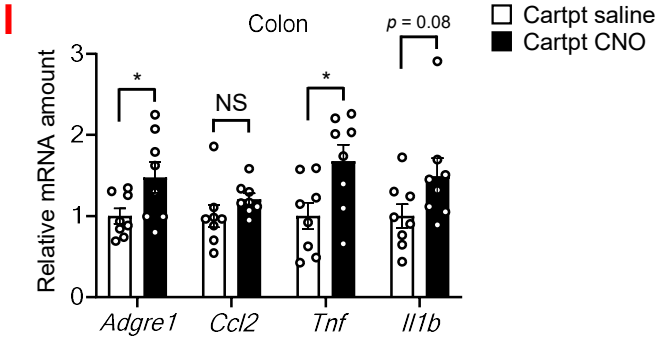
I
Colon
p = 0.08
Cartpt saline
Cartpt CNO
Relative mRNA amount
NS
Adgre1
Ccl2
Tnf
Il1b

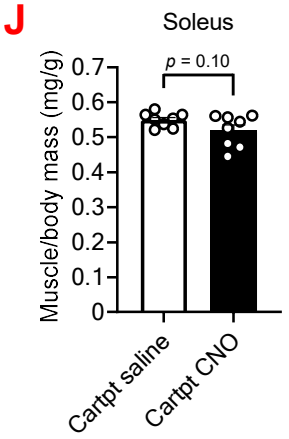
J
Soleus
p = 0.10
Muscle/body mass (mg/g)
Cartpt saline
Cartpt CNO

Figure 6. Sympathetic nerve activation contributes to intestinal inflammation and muscle atrophy induced by limb immobilization

(A and B) NE content (A) and relative NE content (at 4 h versus 0 h) (B) for the stomach, duodenum, proximal and distal small intestine, and colon of control or cast-immobilized (10 days) mice at 0 and 4 h after intraperitoneal (ip) injection of α-MT (n = 6 mice).

(C–H) NE content for the stomach, duodenum, proximal and distal small intestine, and colon (n = 5 mice) (C), the percentage of $CD11c^{+}CD206^{-}$ cells among $CD11b^{+}F4/80^{+}$ cells in the colon (Vehicle control, n = 8; Vehicle IM, n = 6; 6-OHDA control, n = 9; and 6-OHDA IM, n = 6 mice) (D), gut microbial composition at the genus level (Vehicle control, n = 6; Vehicle IM, n = 6; 6-OHDA control, n = 6; and 6-OHDA IM, n = 5 mice) (E), relative abundance of the Lachnospiraceae group (Vehicle control, n = 6; Vehicle IM, n = 6; 6-OHDA control, n = 6; and 6-OHDA IM, n = 5 mice) (F), corresponding principal component analysis (Vehicle control, n = 6; Vehicle IM, n = 6; 6-OHDA control, n = 6; and 6-OHDA IM, n = 5 mice) (G), and ratio of soleus muscle mass to body mass (Vehicle control, n = 11; Vehicle IM, n = 7; 6-OHDA control, n = 11; and 6-OHDA IM, n = 6 mice) (H) of mice subjected to intraperitoneal injection of 6-OHDA or vehicle daily for 3 days, followed (or not) by cast-immobilization for 10 days starting 5 days after the final injection.

(I and J) RT-qPCR analysis of inflammation-related gene expression in the colon (I) and ratio of soleus muscle mass to body mass (J) of *Cartpt-Cre* mice injected with AAV8-*hSyn-DIO-hM3D(Gq)-mCherry* into the lower thoracic spinal cord, followed 3 weeks later by intraperitoneal administration of CNO or saline daily for 7 days (n = 8 mice).

Quantitative data are presented as means ± SEM (A–D and H–J) or medians with interquartile range (F). *$p < 0.05$, **$p < 0.01$, NS by the Mann-Whitney U test (F), the unpaired Student's t test (B, C, I, and J), or two-way ANOVA with the Bonferroni post hoc test (A, D, and H).

Figure 7

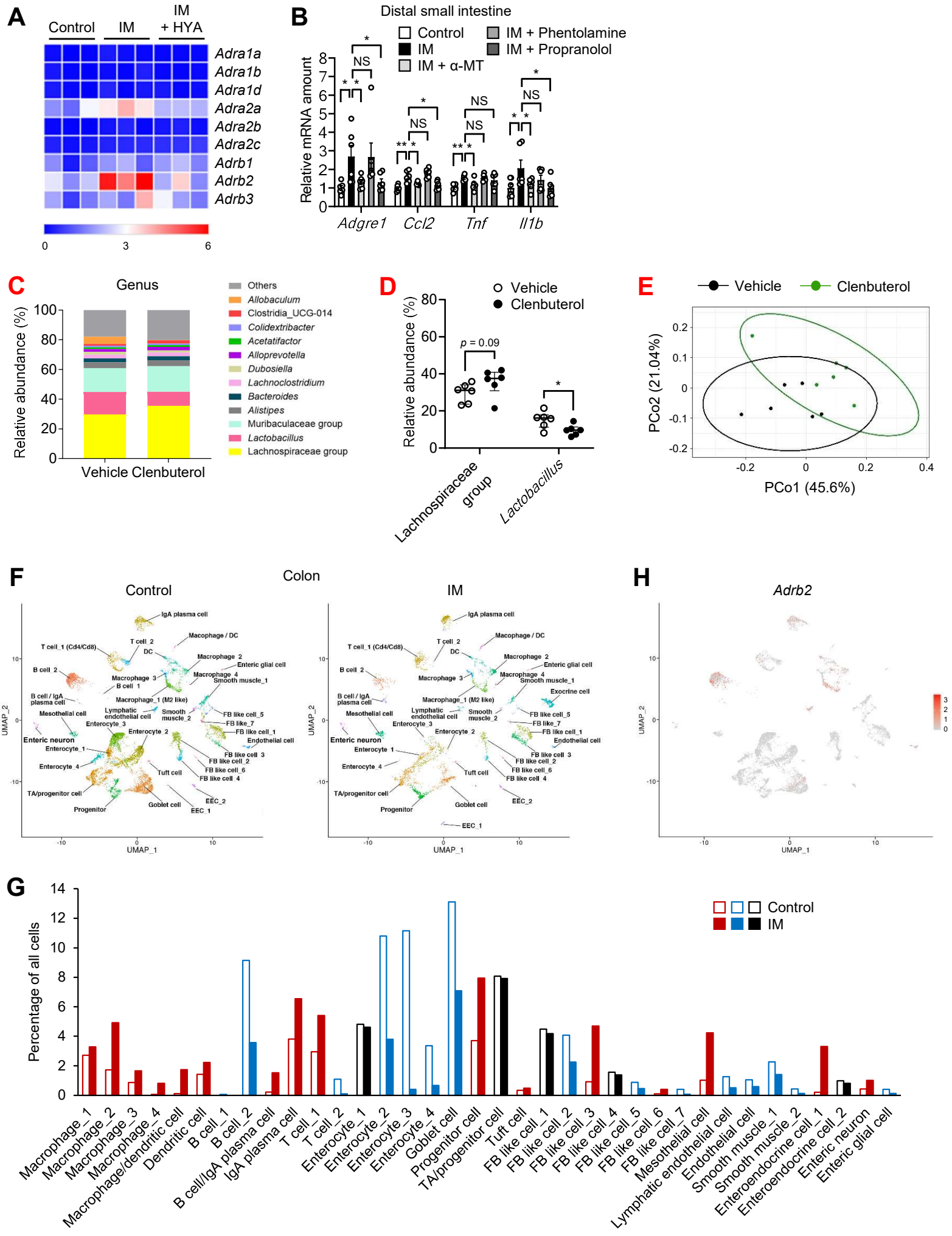
A
Control
IM
IM + HYA
Adra1a
Adra1b
Adra1d
Adra2a
Adra2b
Adra2c
Adrb1
Adrb2
Adrb3
0
3
6
B
Distal small intestine
Control
IM
IM + α-MT
IM + Phentolamine
IM + Propranolol
Relative mRNA amount
NS
Adgre1
Ccl2
Tnf
Il1b
C
Genus
Relative abundance (%)
Vehicle
Clenbuterol
Others
Allobaculum
Clostridia_UCG-014
Colidextribacter
Acetatifactor
Alloprevotella
Dubosiella
Lachnoclostridium
Bacteroides
Alistipes
Muribaculaceae group
Lactobacillus
Lachnospiraceae group
D
Vehicle
Clenbuterol
p = 0.09
Relative abundance (%)
Lachnospiraceae group
Lactobacillus
E
Vehicle
Clenbuterol
PCo2 (21.04%)
PCo1 (45.6%)
F
Colon
Control
IM
UMAP_1
UMAP_2
H
Adrb2
G
Percentage of all cells
Control
IM
Macrophage_1
Macrophage_2
Macrophage_3
Macrophage_4
Macrophage/dendritic cell
Dendritic cell
B cell_1
B cell_2
B cell/IgA plasma cell
IgA plasma cell
T cell_1
T cell_2
Enterocyte_1
Enterocyte_2
Enterocyte_3
Enterocyte_4
Goblet cell
Progenitor cell
TA/progenitor cell
Tuft cell
FB like cell_1
FB like cell_2
FB like cell_3
FB like cell_4
FB like cell_5
FB like cell_6
FB like cell_7
Mesothelial cell
Lymphatic endothelial cell
Endothelial cell
Smooth muscle_1
Smooth muscle_2
Enteroendocrine cell_1
Enteroendocrine cell_2
Enteric neuron
Enteric glial cell

Figure 7. Sympathetic nerve activation contributes to immobilization-induced intestinal inflammation and dysbiosis via the activation of Adrb2 signaling

(A) Heat map for the expression of adrenergic receptor genes in the colon of mice fed a normal diet or a diet containing HYA and subjected (or not) to cast-immobilization for 10 days (n = 3 mice).

(B) RT-qPCR analysis of inflammation-related gene expression in the distal small intestine of mice subjected to intraperitoneal injection of α-MT, phentolamine, propranolol, or vehicle daily for 10 days with or without concomitant cast-immobilization (n = 6 mice).

(C–E) Gut microbial composition at the genus level (C), relative abundance of the Lachnospiraceae group and *Lactobacillus* species (D), and corresponding principal coordinate analysis (E) of mice subjected to intraperitoneal injection of clenbuterol or vehicle daily for 10 days (n = 6 mice).

(F) Uniform manifold approximation and projection (UMAP) representation of 37 cell clusters identified by scRNA-seq analysis of the colon for control mice or mice subjected to cast-immobilization for 10 days. DC, dendritic cell; EEC, enteroendocrine cell; FB, fibroblast.

(G) Percentage of the indicated cell clusters among all cells. Red or blue squares indicate cell clusters for which cast-immobilization increased or decreased the cell ratio by >20%, respectively.

(H) Feature plot of *Adrb2* expression in the cell clusters of the colon.

Quantitative data are presented as means ± SEM (B) or medians with interquartile range (D). *$p < 0.05$, **$p < 0.01$, NS by the Mann-Whitney U test (D) or two-way ANOVA with the Bonferroni post hoc test (B).

Figure 8

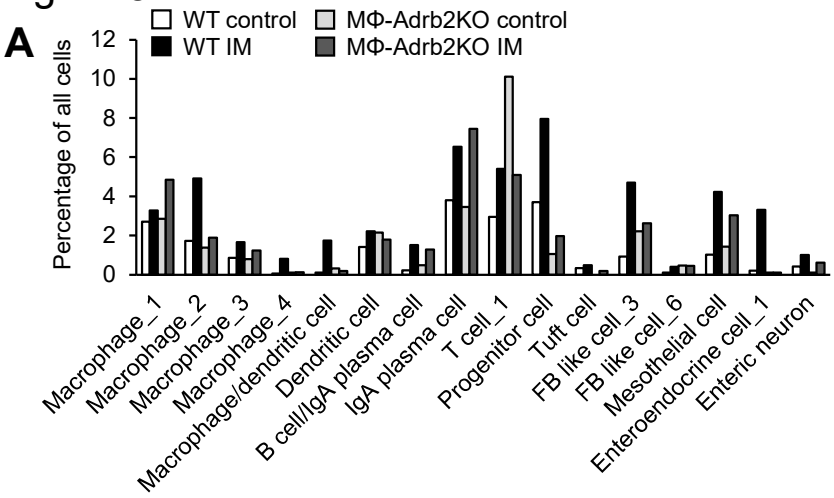
A
WT control
WT IM
MΦ-Adrb2KO control
MΦ-Adrb2KO IM
Percentage of all cells
Macrophage_1
Macrophage_2
Macrophage_3
Macrophage_4
Macrophage/dendritic cell
Dendritic cell
B cell/IgA plasma cell
IgA plasma cell
T cell_1
Progenitor cell
Tuft cell
FB like cell_3
FB like cell_6
Mesothelial cell
Enteroendocrine cell_1
Enteric neuron

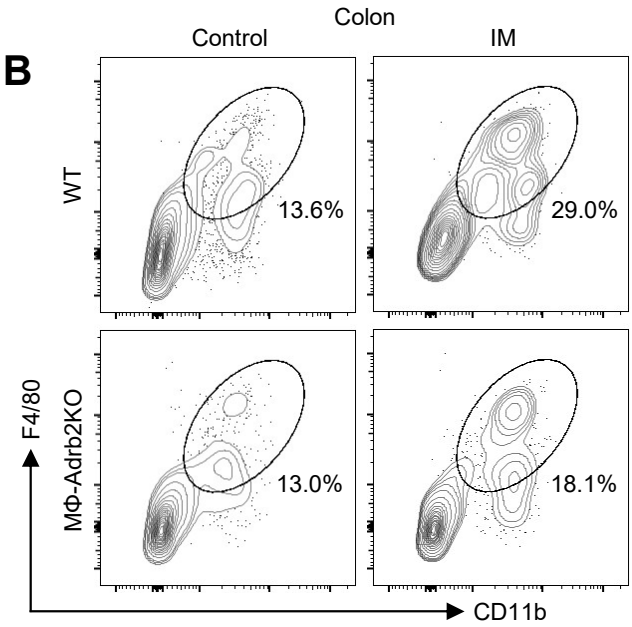
B
Colon
Control
IM
WT
MΦ-Adrb2KO
13.6%
29.0%
13.0%
18.1%
F4/80
CD11b

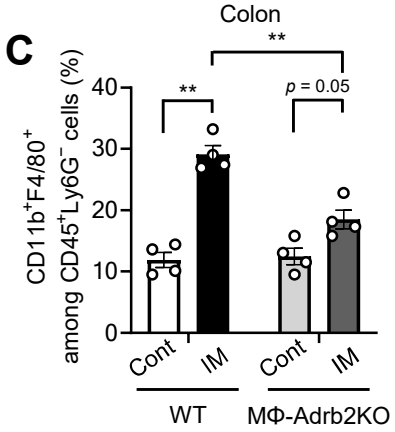
C
Colon
CD11b+F4/80+ among CD45+Ly6G− cells (%)
p = 0.05
Cont
IM
WT
MΦ-Adrb2KO

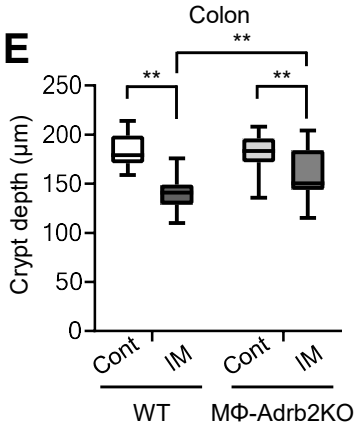
E
Colon
Crypt depth (μm)
Cont
IM
WT
MΦ-Adrb2KO

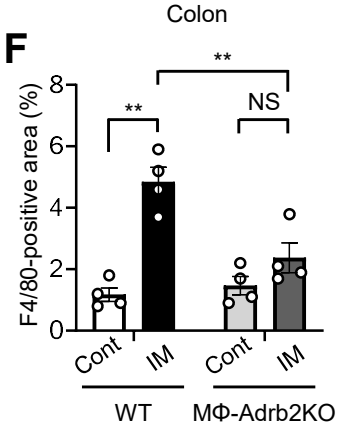
F
Colon
F4/80-positive area (%)
NS
Cont
IM
WT
MΦ-Adrb2KO

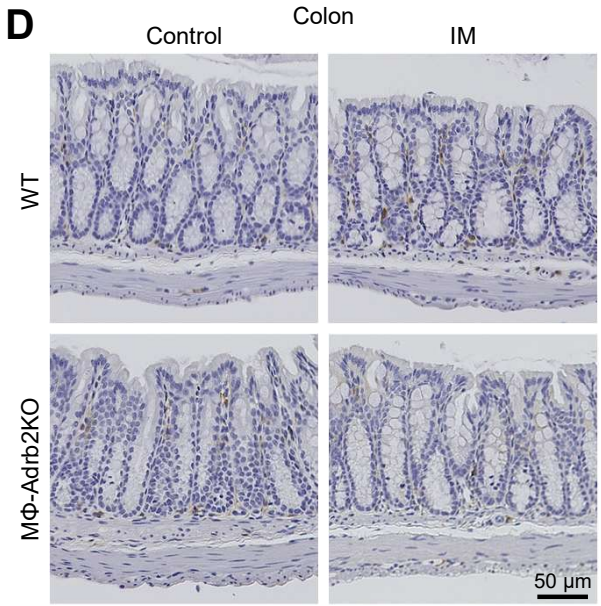
D
Colon
Control
IM
WT
MΦ-Adrb2KO
50 μm

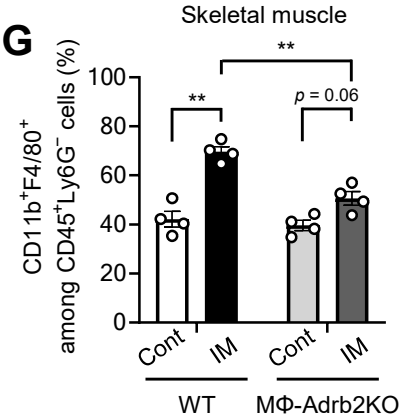
G
Skeletal muscle
CD11b+F4/80+ among CD45+Ly6G− cells (%)
p = 0.06
Cont
IM
WT
MΦ-Adrb2KO

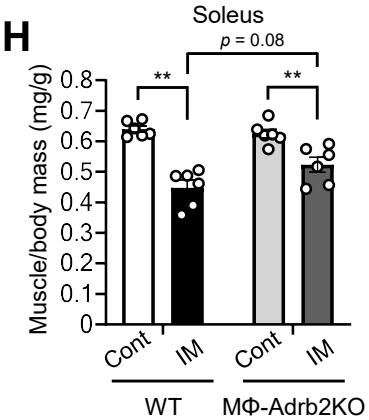
H
Soleus
p = 0.08
Muscle/body mass (mg/g)
Cont
IM
WT
MΦ-Adrb2KO

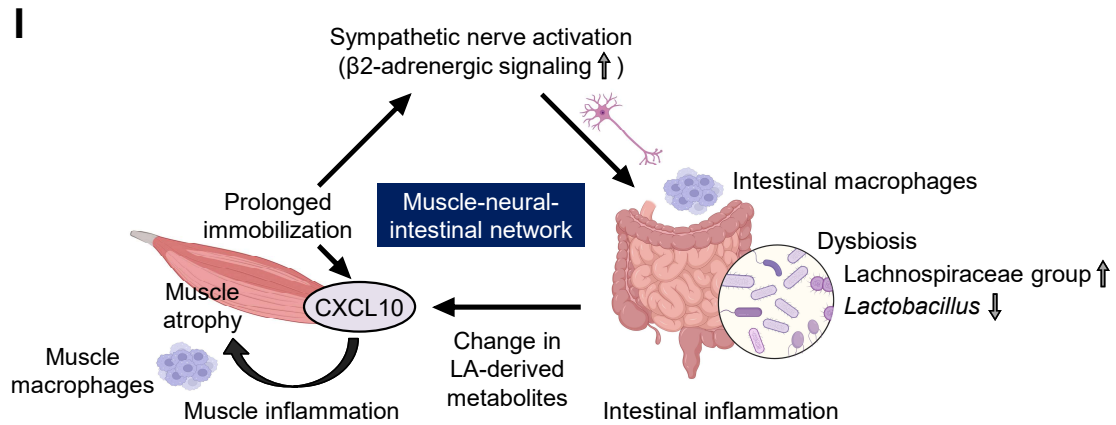
I
Sympathetic nerve activation
(β2-adrenergic signaling ⇧)
Prolonged immobilization
Muscle-neural-intestinal network
Intestinal macrophages
Dysbiosis
Lachnospiraceae group ⇧
Lactobacillus ⇩
Muscle atrophy
CXCL10
Muscle macrophages
Muscle inflammation
Change in LA-derived metabolites
Intestinal inflammation

Figure 8. Prevention of β2-adrenergic signaling in macrophages attenuates intestinal and muscle inflammation induced by prolonged limb immobilization

(A–H) Percentage of the indicated cell clusters among all cells in the colon as determined by scRNA-seq analysis (A); representative flow cytometric analysis (B) and the percentage (*n* = 4 mice) (C) of $CD11b^{+}F4/80^{+}$ cells among $CD45^{+}Ly6G^{-}$ cells in the colon; F4/80 immunohistochemical staining of the colon (D) for determination of crypt depth (*n* = 4 mice) (E) and the F4/80-positive area (*n* = 4 mice) (F); the percentage of $CD11b^{+}F4/80^{+}$ cells among $CD45^{+}Ly6G^{-}$ cells in hind limb skeletal muscle (*n* = 4 mice) (G); and the ratio of soleus muscle mass to body mass (*n* = 6 mice) (H) for wild-type (WT) or macrophage-specific Adrb2 KO (MΦ-Adrb2KO) mice subjected (or not) to cast-immobilization for 10 days. The depth of 100 crypts pooled from four mice was measured and averaged for each condition in (E). Scale bar (D), 50 μm. (I) Proposed role of a skeletal muscle–sympathetic nerve–intestine network in immobilization-induced muscle inflammation and atrophy. Quantitative data are presented as means ± SEM (C and F–H) or medians with interquartile range (E). $^{**}p < 0.01$, NS (two-way ANOVA with the Bonferroni post hoc test).

Supplemental Figure 1

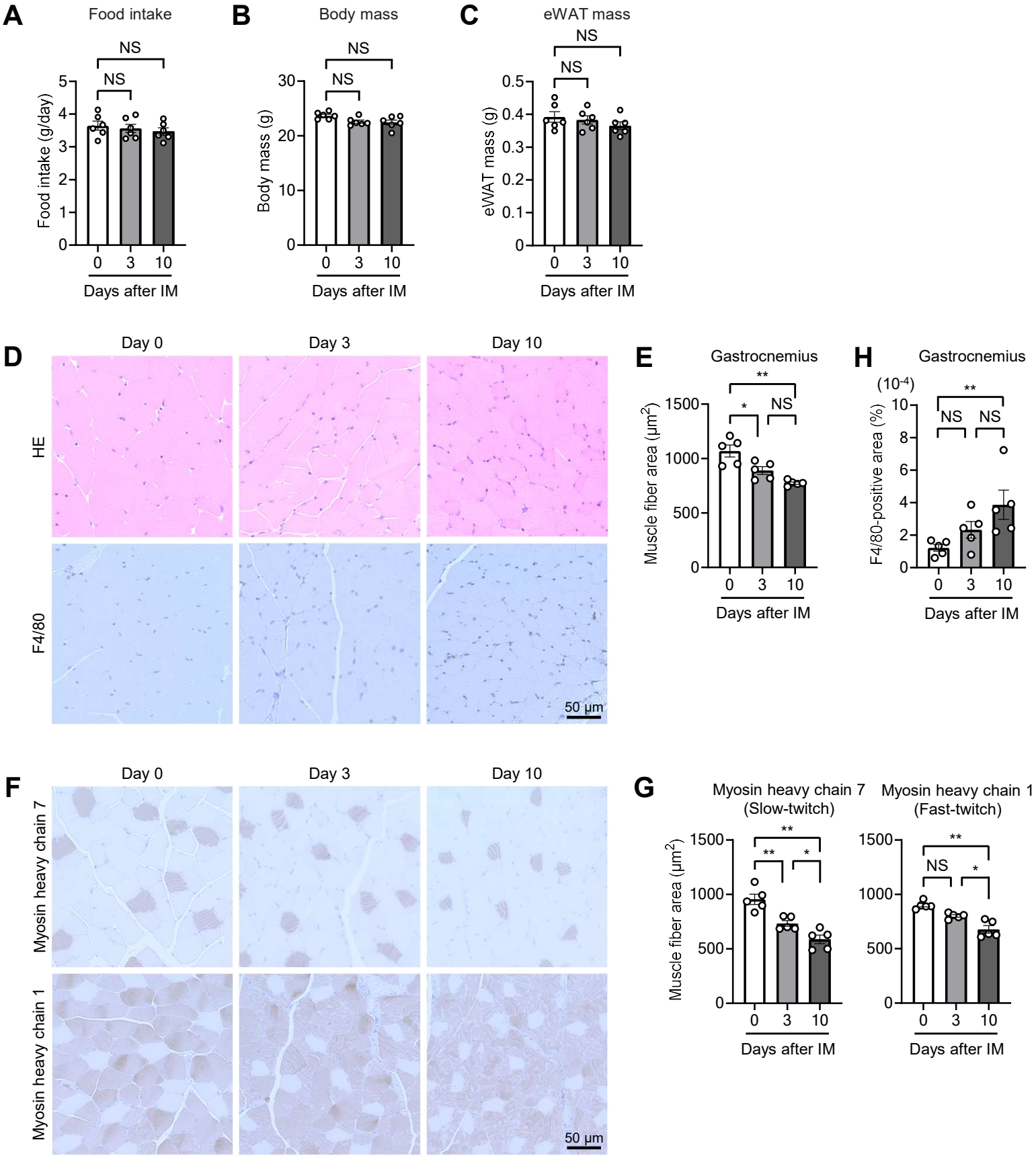

Figure S1. Hematoxylin-eosin staining and immunohistochemical staining in skeletal muscle of immobilized mice

(A–C) Daily food intake (A), body mass (B), and epididymal white adipose tissue (eWAT) mass (C) for mice subjected to bilateral hind limb immobilization by cast-fixation for the indicated times (n = 6 mice).

(D and E) Hematoxylin-eosin staining and immunohistochemical staining of F4/80 (D) for determination of muscle fiber area (E) in gastrocnemius muscle of mice subjected to hind limb immobilization for the indicated times (n = 5 mice). The area of fibers pooled from five mice was measured and averaged for each condition in (E). Scale bar (D), 50 μm.

(F and G) Immunohistochemical staining of myosin heavy chain 7 and myosin heavy chain 1 (F) for determination of muscle fiber area (G) in gastrocnemius muscle of mice subjected to hind limb immobilization for the indicated times (n = 5 mice). The area of fibers pooled from five mice was measured and averaged for each condition in (G). Scale bar (F), 50 μm.

(H) The F4/80-positive area in gastrocnemius muscle of mice subjected to hind limb immobilization for the indicated times (n = 5 mice).

Quantitative data are presented as means ± SEM (A–C, E, G, and H). *$p < 0.05$, **$p < 0.01$, NS by two-way ANOVA with the Bonferroni post hoc test.

Supplemental Figure 2

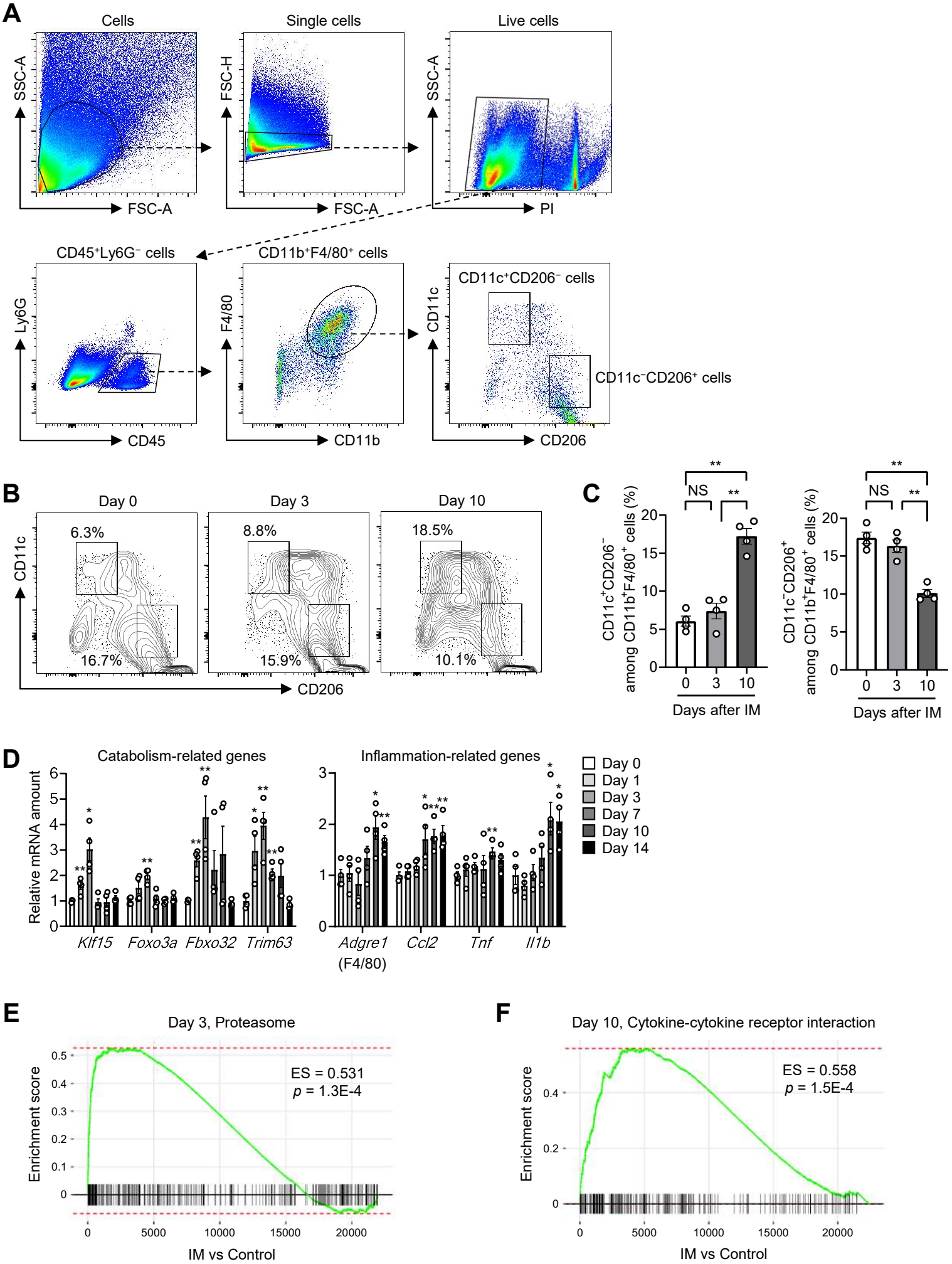

Figure S2. Gating strategy and immobilization-induced changes in macrophage subsets of skeletal muscle as well as GSEA for immobilized muscle

(A) Gating strategy for fluorescence-activated sorting of macrophages from skeletal muscle of immobilized mice. SSC, side scatter; FSC, forward scatter; PI, propidium iodide.

(B and C) Representative flow cytometric analysis (B) and the percentage (C) of $CD11c^{+}CD206^{-}$ or $CD11c^{-}CD206^{+}$ cells in skeletal muscle of mice subjected to hind limb immobilization by cast-fixation for the indicated times (n = 4 mice).

(D) RT-qPCR analysis of protein catabolism– or inflammation-related gene expression in soleus muscle of immobilized mice (n = 4 mice).

(E and F) GSEA for the indicated pathways performed with RNA-seq data from gastrocnemius muscle of mice immobilized for 3 days (E) or 10 days (F). ES, enrichment score.

Quantitative data are presented as means ± SEM (C and D). *$p < 0.05$, **$p < 0.01$, NS compared with day 0 (D) or as indicated (C) by two-way ANOVA with the Bonferroni post hoc test.

Supplemental Figure 3

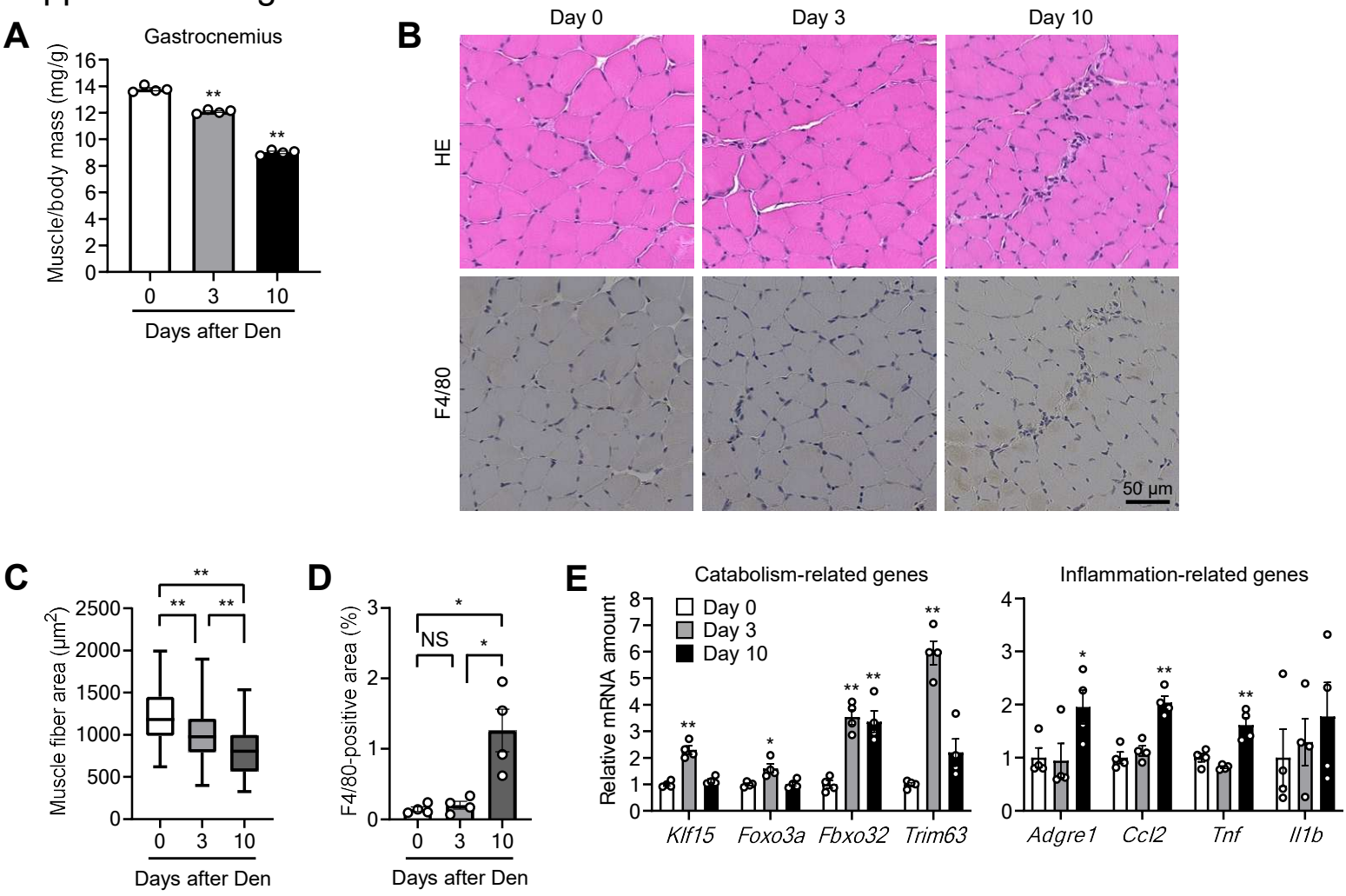

Figure S3. Time course of denervation-induced muscle atrophy, macrophage accumulation, and changes in gene expression

(A) Ratio of gastrocnemius muscle mass in both hind limbs to body mass for mice subjected to bilateral hind limb denervation (Den) for the indicated times (n = 4 mice).

(B–D) Hematoxylin-eosin and F4/80 immunohistochemical staining (B) for determination of muscle fiber area (C) and the F4/80-positive area (D) in soleus muscle of denervated mice (n = 4 mice). The area of 800 fibers pooled from four mice was measured and averaged for each condition in (C). Scale bar (B), 50 μm.

(E) RT-qPCR analysis of protein catabolism– or inflammation-related gene expression in the gastrocnemius of denervated mice (n = 4 mice).

Quantitative data are presented as means ± SEM (A, D, and E) or medians with interquartile range (C). *$p < 0.05$, **$p < 0.01$, NS compared with day 0 (A and E) or as indicated (C and D) by two-way ANOVA with the Bonferroni post hoc test.

Supplemental Figure 4

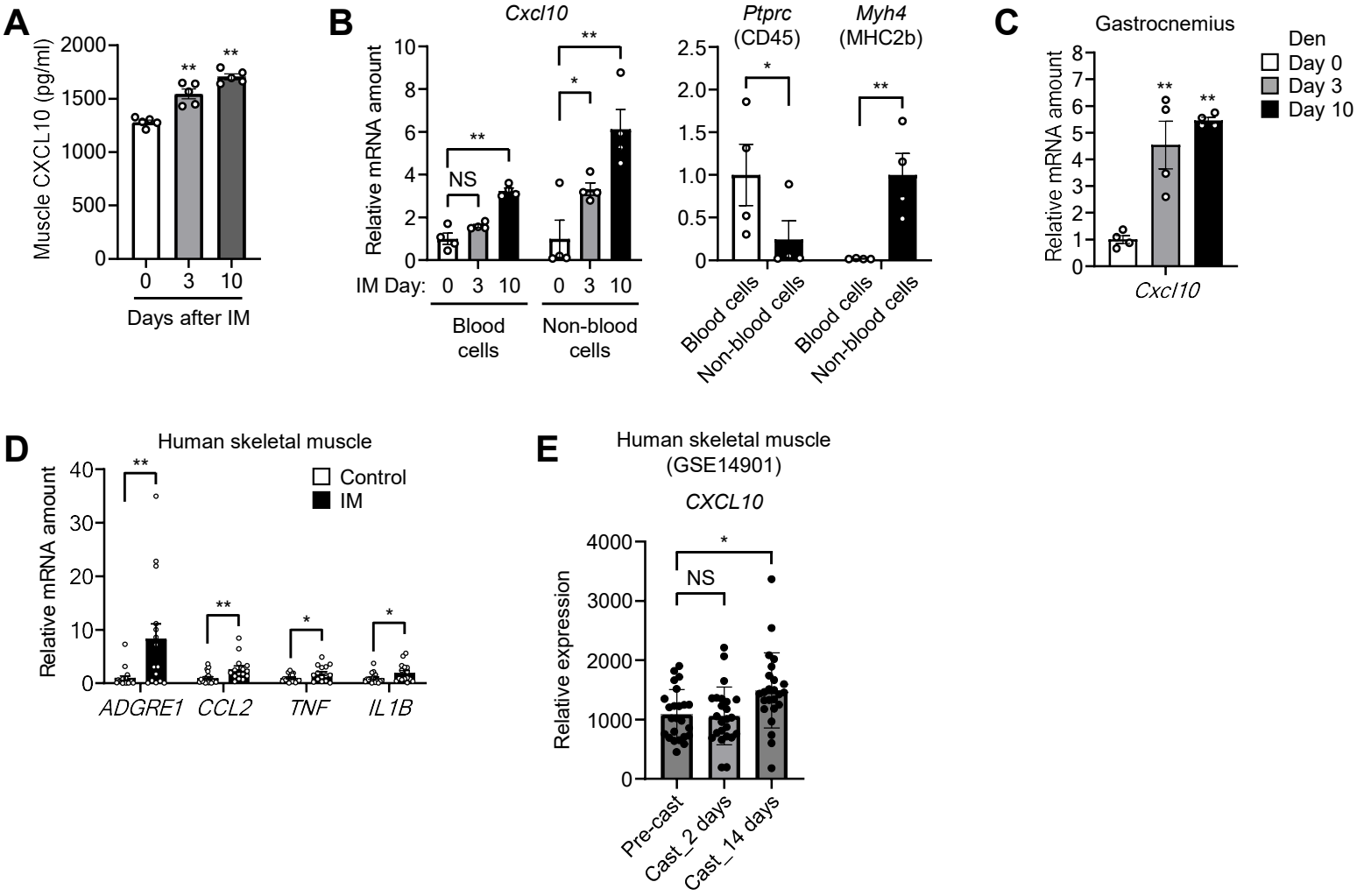

Figure S4. Identification of the chemokine CXCL10 as a mediator of muscle inflammation induced by limb immobilization

(A) Muscle tissue concentration of CXCL10 in cast-immobilized mice (*n* = 5 mice).

(B) RT-qPCR analysis of *Cxcl10*, *Ptprc*, and *Myh4* mRNA abundance in the blood cell and non–blood cell fractions of skeletal muscle from cast-immobilized mice (*n* = 4 mice).

(C) RT-qPCR analysis of *Cxcl10* mRNA in gastrocnemius of denervated mice (*n* = 4 mice).

(D) RT-qPCR analysis of inflammation-related gene expression in skeletal muscle of control (*n* = 18) or immobilized (*n* = 15) human participants.

(E) Relative expression of *CXCL10* in skeletal muscle of healthy human individuals subjected to cast-immobilization as determined from a publicly available data set. The relative expression level is presented as transcripts per million (TPM) for the subjects before (Pre-cast) and at two time points after (Cast_2 days and Cast_14 days) cast application. Each point represents one individual.

Quantitative data are presented as means ± SEM (A–E). *$p < 0.05$, **$p < 0.01$, NS compared with day 0 (A and C) or as indicated (B, D, and E) by the unpaired Student's *t* test (B and D), two-way ANOVA with the Bonferroni post hoc test (A–C), or one-way ANOVA followed by Dunnett's test (E).

Supplemental Figure 5

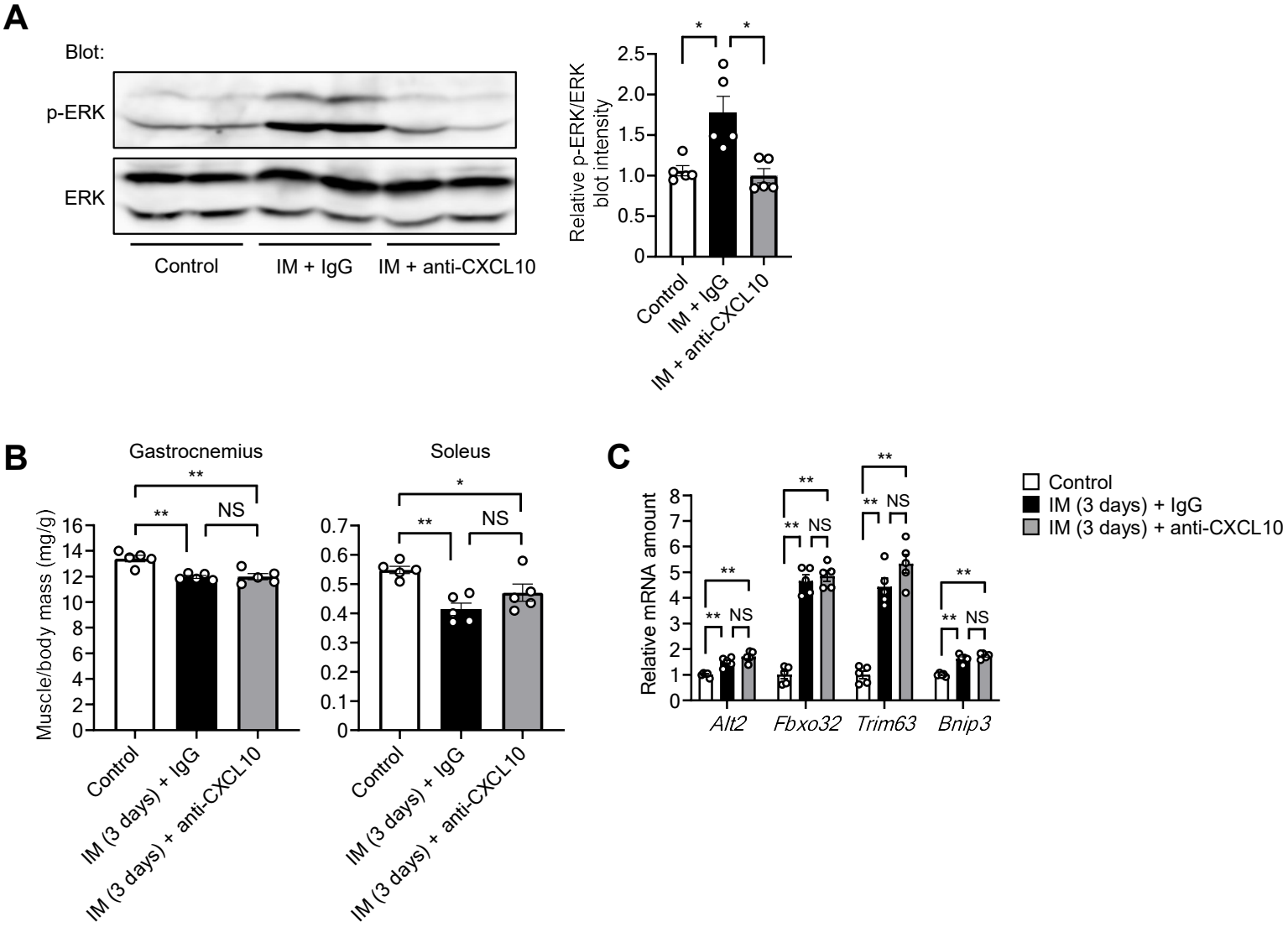

Figure S5. Effects of neutralizing antibodies to CXCL10 on muscle inflammation and atrophy induced by immobilization

(A) Immunoblot analysis of total and phosphorylated (p-) forms of ERK in gastrocnemius for control mice or mice subjected to intraperitoneal injection of neutralizing antibodies to CXCL10 (0.1 mg/body) or control IgG 3 days before cast-immobilization for 10 days (n = 5 mice).

(B and C) Ratio of muscle mass to body mass (B) and RT-qPCR analysis of catabolism-related gene expression in gastrocnemius (C) for control mice or mice subjected to intraperitoneal injection of neutralizing antibodies to CXCL10 (0.1 mg/body) or control IgG 3 days before cast-immobilization for 3 days (*n* = 5 mice).

Quantitative data are presented as means ± SEM (A–C). *$p < 0.05$, **$p < 0.01$, NS by two-way ANOVA with the Bonferroni post hoc test.

Supplemental Figure 6

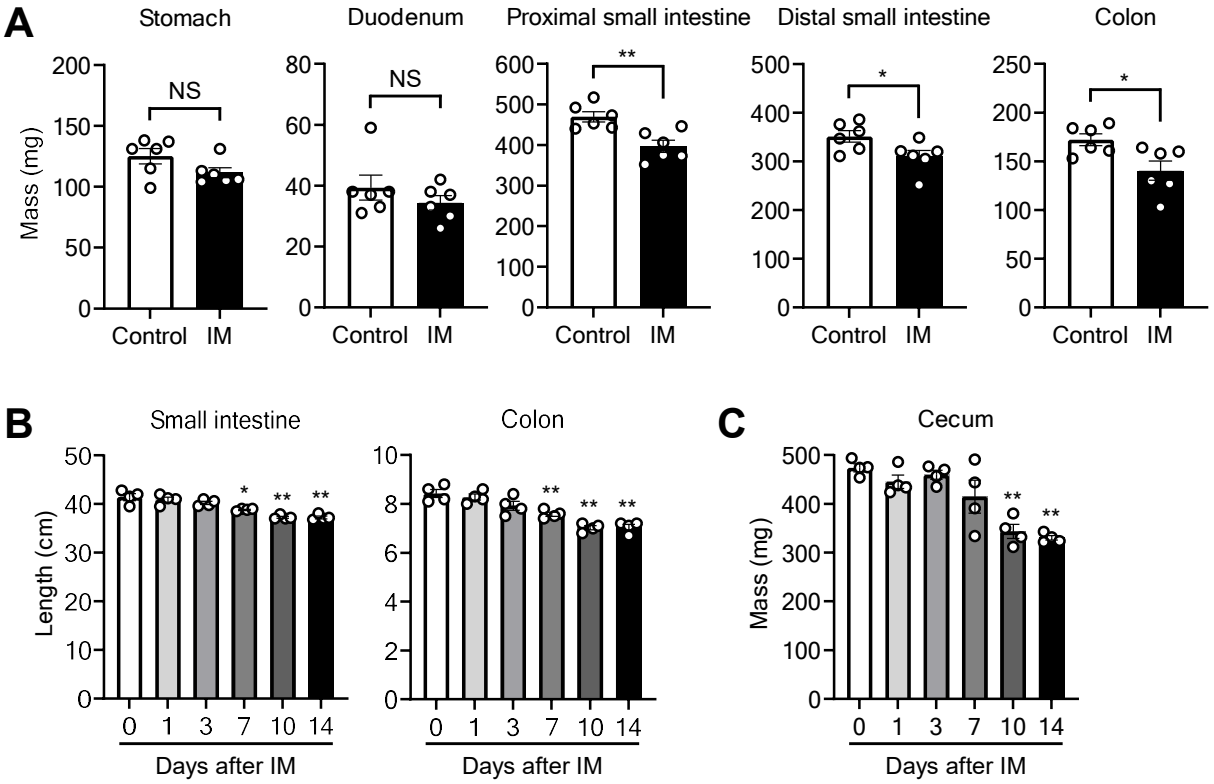

Figure S6. Effects of prolonged limb immobilization on intestinal tissue
(A) Mass of the stomach, duodenum, proximal and distal small intestine, and colon for control mice or mice subjected to cast-immobilization for 10 days (n = 6 mice).
(B and C) Length of the small intestine and colon (B) as well as mass of the cecum (C) for mice subjected to cast-immobilization for the indicated times (n = 4 mice).
Quantitative data are presented as means ± SEM (A–C). *$p < 0.05$, **$p < 0.01$, NS compared with day 0 (B and C) or as indicated (A) by the unpaired Student's t test (A) or two-way ANOVA with the Bonferroni post hoc test (B and C).

Supplemental Figure 7

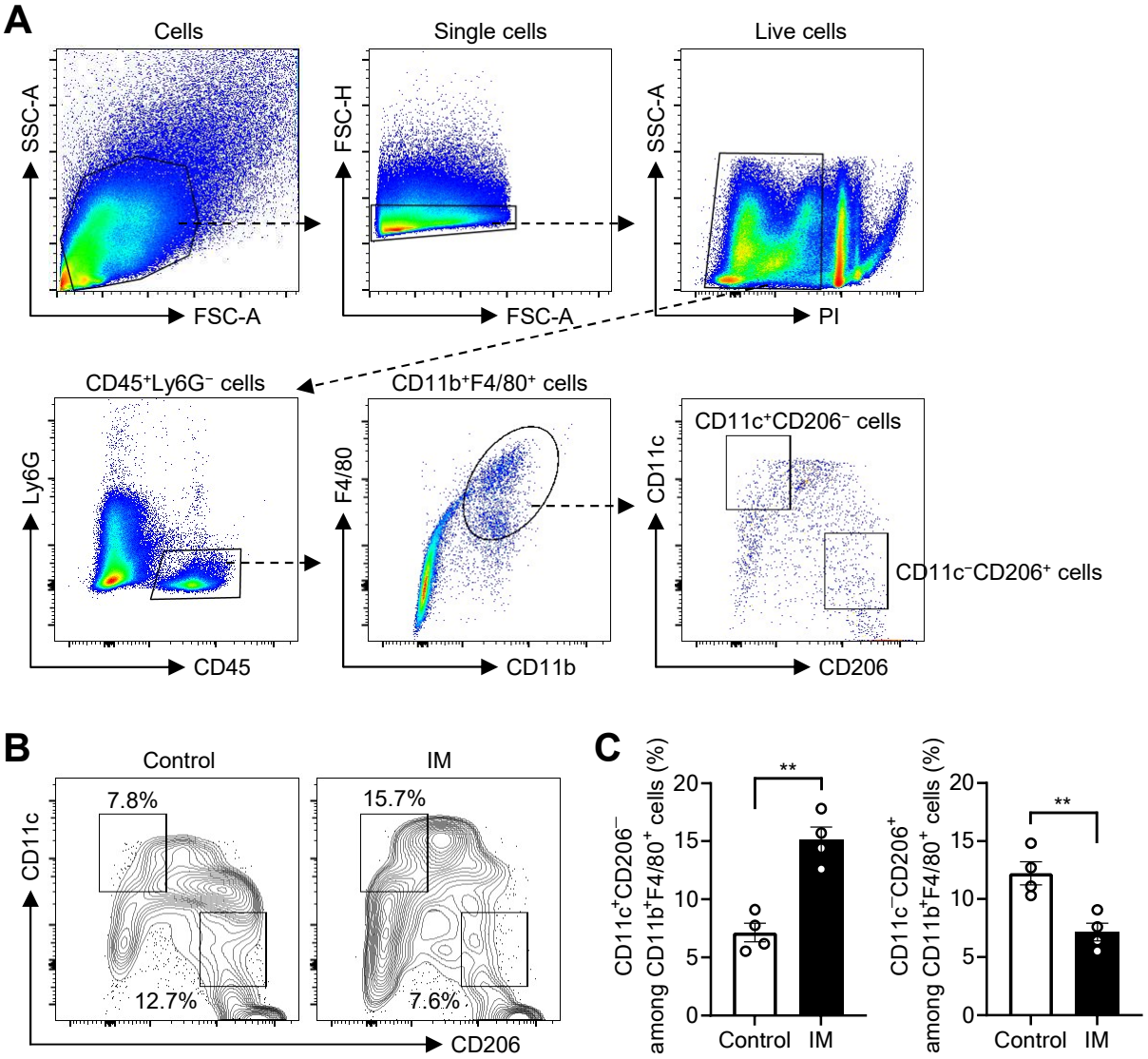

Figure S7. Gating strategy for macrophage subsets in the colon

(A) Gating strategy for fluorescence-activated sorting of macrophages from the colon of immobilized mice.

(B and C) Representative flow cytometric analysis (B) and the percentage (C) of $CD11c^{+}CD206^{-}$ or $CD11c^{-}CD206^{+}$ cells in the colon of cast-immobilized (10 days) and control mice (n = 4 mice).

Quantitative data are presented as means ± SEM (C). $^{**}p < 0.01$ by the unpaired Student's t test.

Supplemental Figure 8

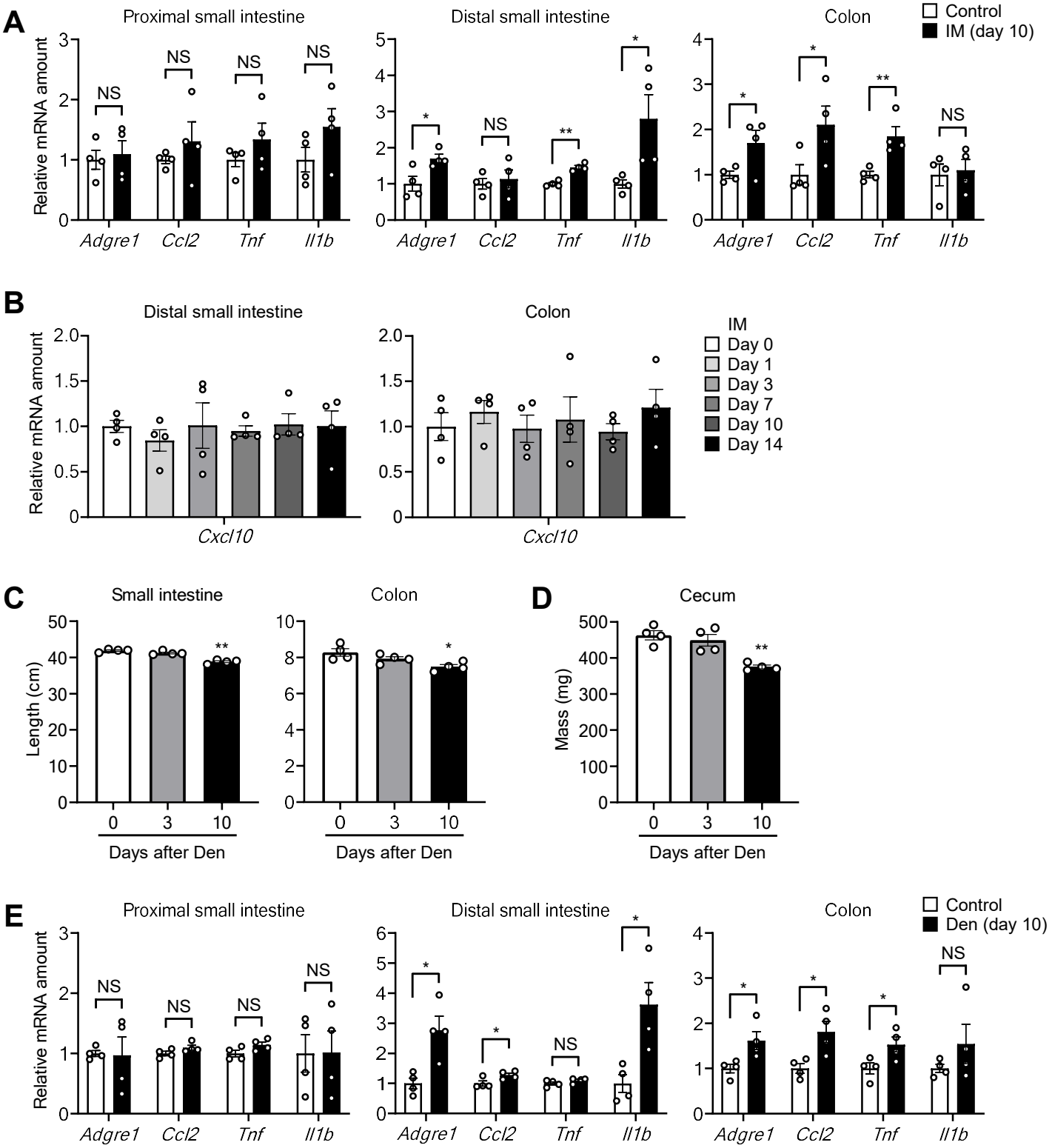

Figure S8. Effects of prolonged limb immobilization by cast-fixation or denervation on intestinal tissue

(A) RT-qPCR analysis of inflammation-related gene expression in the proximal or distal small intestine and colon of cast-immobilized (10 days) and control mice (n = 4 mice).

(B) RT-qPCR analysis of *Cxcl10* mRNA abundance in the distal small intestine and colon of cast-immobilized mice (n = 4 mice).

(C and D) Length of the small intestine and colon (C) as well as mass of the cecum (D) for mice subjected to limb denervation for the indicated times (n = 4 mice).

(E) RT-qPCR analysis of inflammation-related gene expression in the proximal or distal small intestine and colon of denervated and control mice (n = 4 mice).

Quantitative data are presented as means ± SEM (A–E). *$p < 0.05$, **$p < 0.01$, NS compared with day 0 (B–D) or as indicated (A and E) by the unpaired Student's t test (A and E) or two-way ANOVA with the Bonferroni post hoc test (B–D).

Supplemental Figure 9

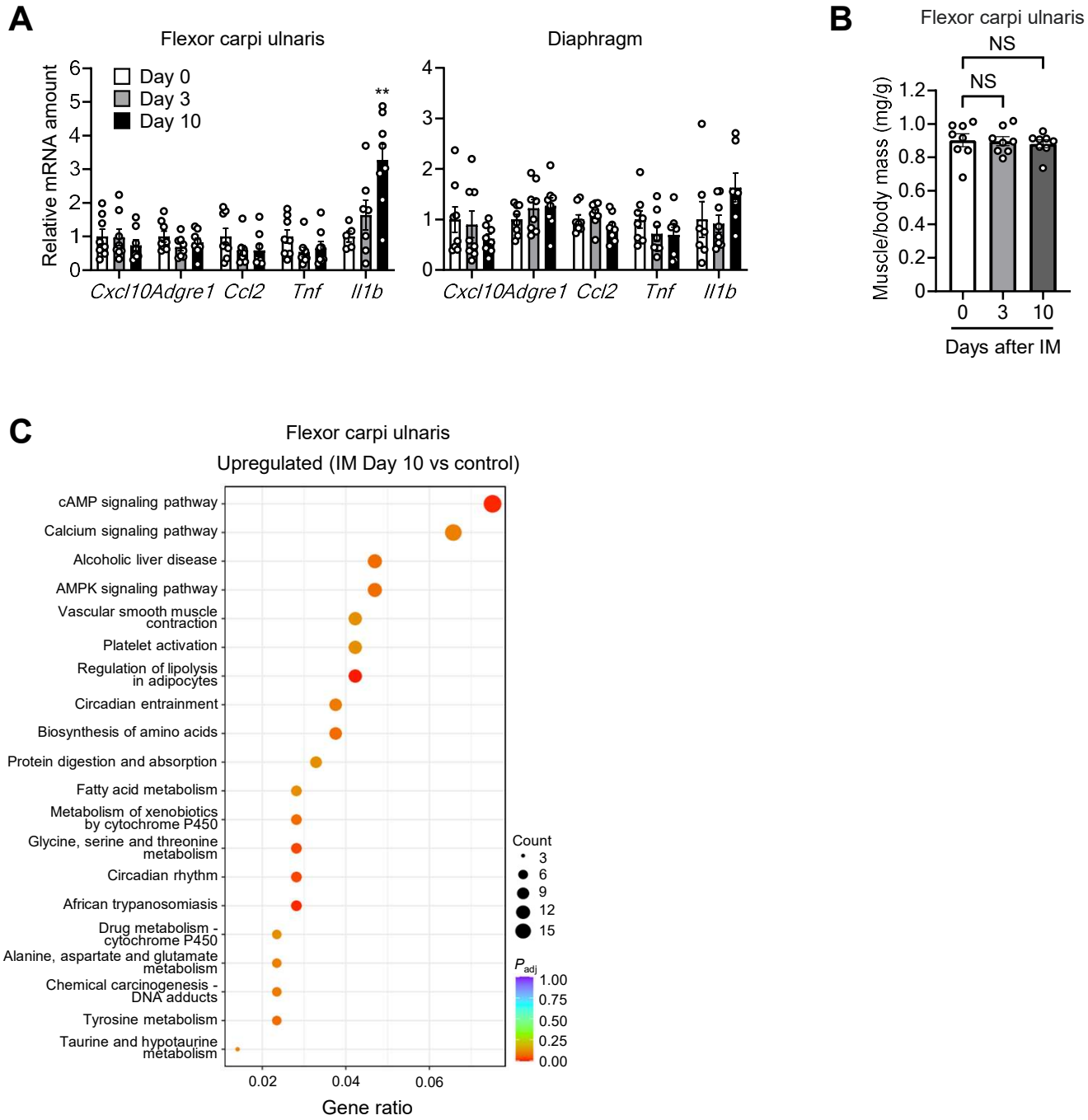

Figure S9. Time course of muscle mass and changes in gene expression in non-immobilized muscles

(A) RT-qPCR analysis of inflammation-related gene expression in flexor carpi ulnaris and diaphragm of immobilized mice (n = 8 mice).

(B) Ratio of flexor carpi ulnaris mass to body mass for mice subjected to cast-immobilization for the indicated times (n = 8 mice).

(C) KEGG pathway analysis for RNA-seq data from flexor carpi ulnaris at 10 days after hind limb immobilization. The top 20 pathways enriched among genes whose expression was upregulated by immobilization are shown. p_{adj}, adjusted p value.

Quantitative data are presented as means ± SEM (A and B). **p < 0.01, NS compared with day 0 (A) or as indicated (B) by two-way ANOVA with the Bonferroni post hoc test.

Supplemental Figure 10

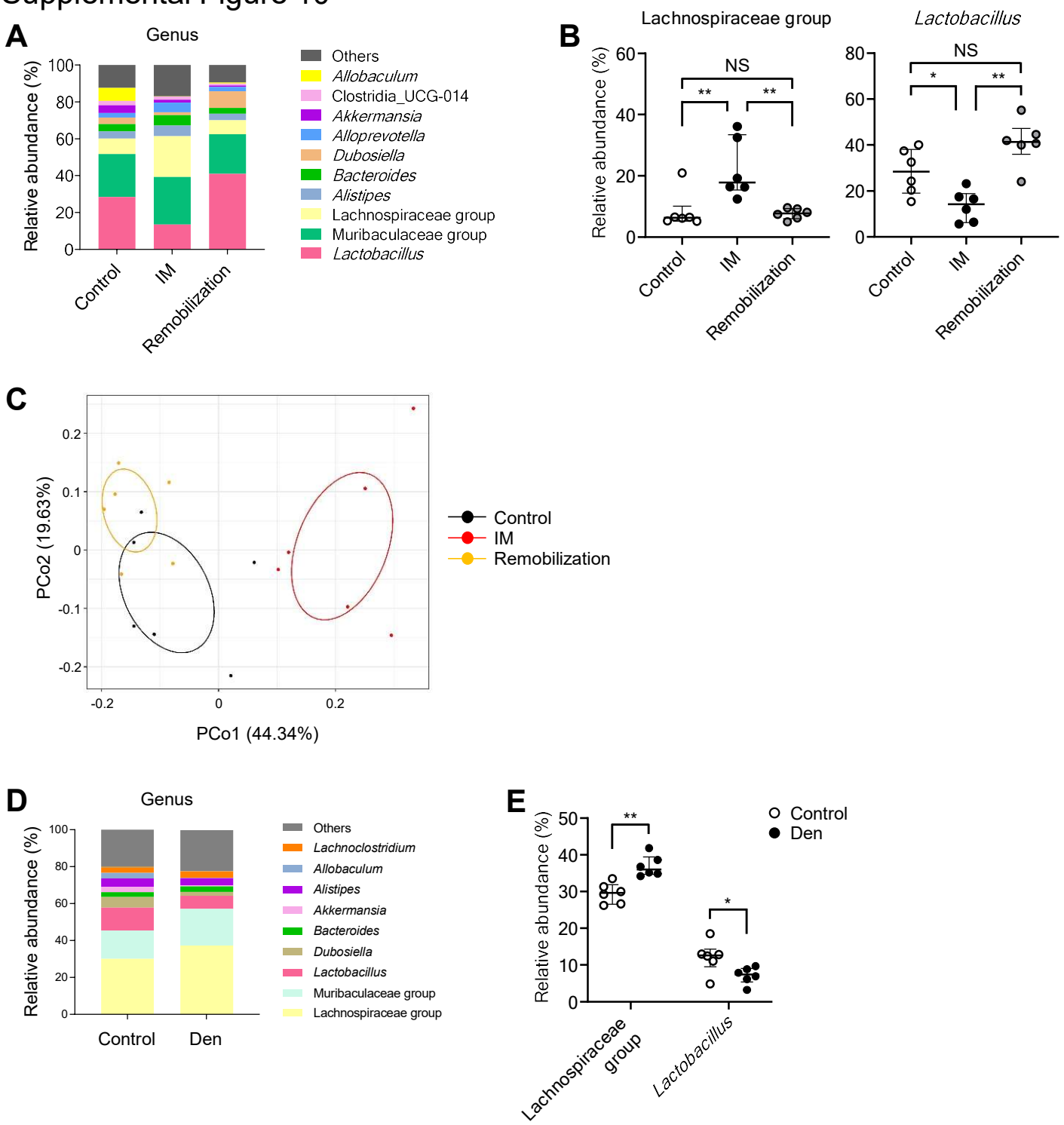

Figure S10. Effects of prolonged limb immobilization by cast-fixation or denervation on the gut microbiota

(A–C) Gut microbial composition at the genus level (A), relative abundance of the Lachnospiraceae group and *Lactobacillus* species (B), and corresponding principal coordinate analysis (C) for control mice and mice subjected to cast immobilization for 10 days with (remobilization) or without subsequent cast removal for 14 days (n = 6 mice).
(D and E) Gut microbial composition at the genus level (D) and relative abundance of the Lachnospiraceae group and *Lactobacillus* species (E) for control mice or mice subjected to hind limb denervation for 10 days (n = 6 mice).
Quantitative data are presented as medians with interquartile range (B and E). *$p < 0.05$, **$p < 0.01$, NS by the Mann-Whitney U test (E), one-way ANOVA with the Bonferroni post hoc test (B).

Supplemental Figure 11

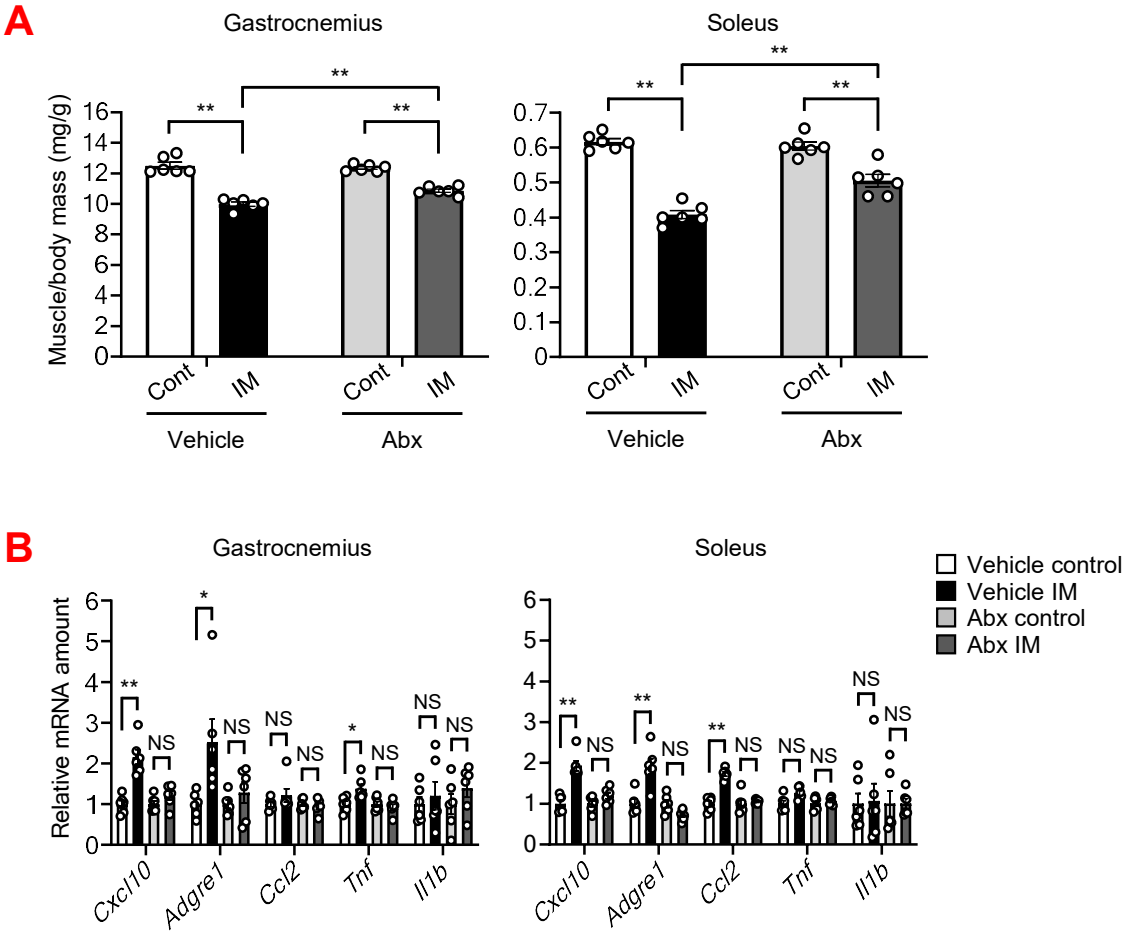

Figure S11. Effects of pseudosterilization of the intestine by antibiotics on muscle inflammation and atrophy induced by immobilization

(A and B) Ratio of gastrocnemius and soleus muscle mass to body mass (A), and RT-qPCR analysis of inflammation-related gene expression in gastrocnemius and soleus (B) of mice treated with a cocktail of antibiotics (Abx) or vehicle by oral gavage daily from 4 days before immobilization, with or without cast-immobilization for 10 days (n = 6 mice). Quantitative data are presented as means ± SEM. *$p < 0.05$, **$p < 0.01$, NS by two-way ANOVA with the Bonferroni post hoc test.

Supplemental Figure 12

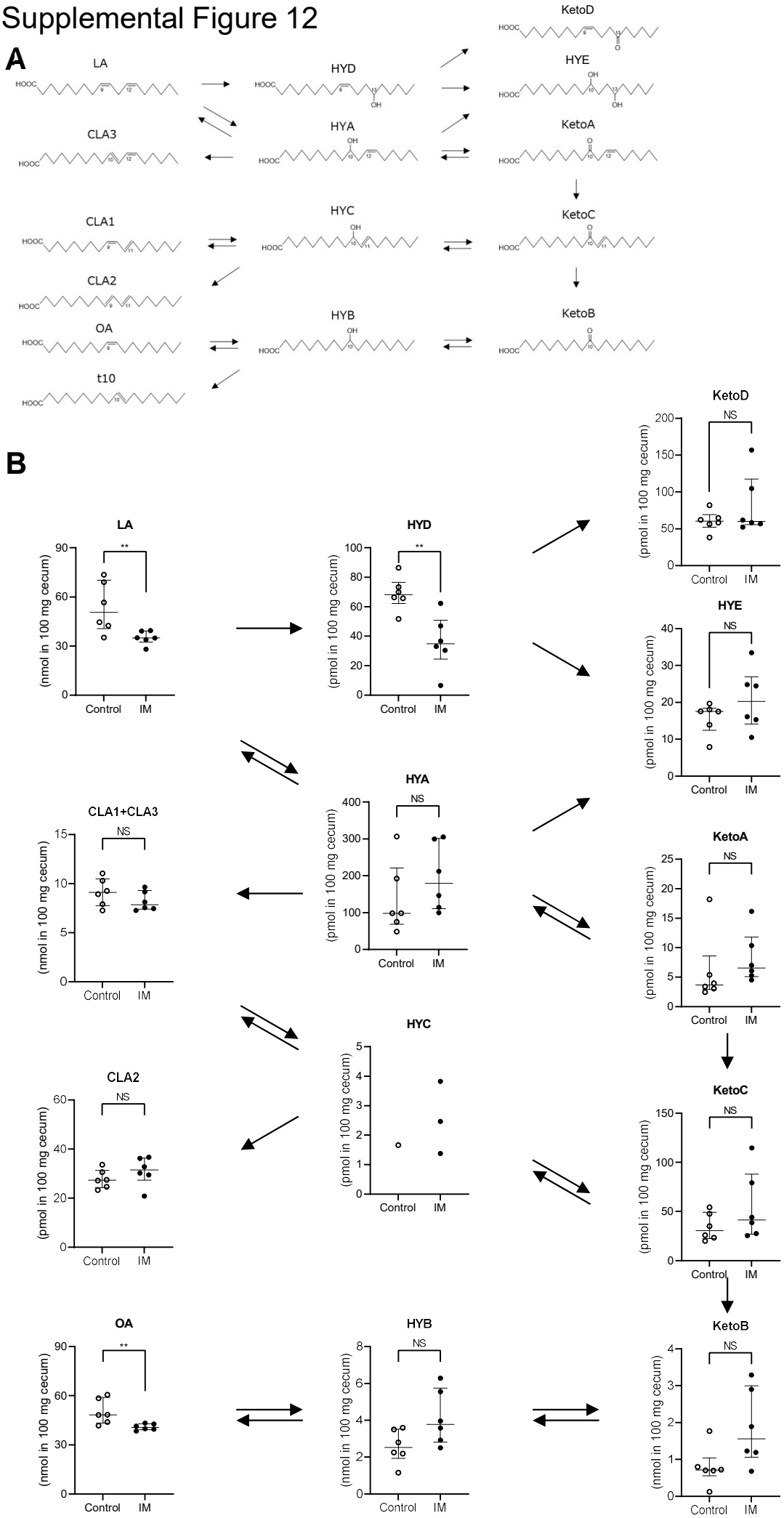

Figure S12. Prolonged limb immobilization by cast-fixation influences the fecal levels of fatty acid metabolites produced by the gut microbiota

(A) Metabolic pathway of LA showing the structure of fatty acid metabolites.

(B) Fatty acid concentrations in cecal content of mice subjected (or not) to cast-immobilization for 10 days (n = 6 mice). HYC was below the detection limit in most samples. Quantitative data are presented as medians with interquartile range (B). $^{**}p < 0.01$, NS by the Mann-Whitney U test.

Supplemental Figure 13

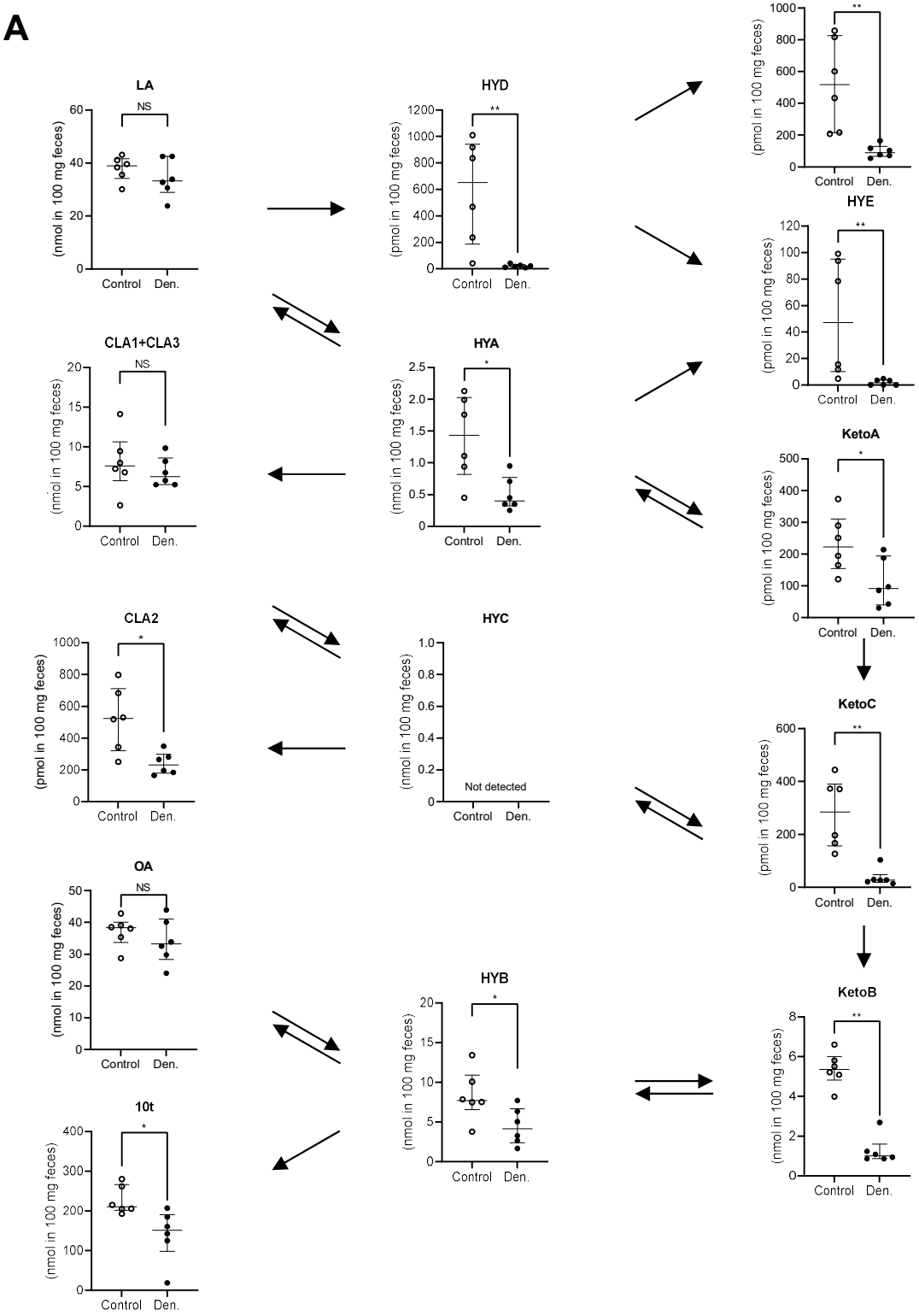

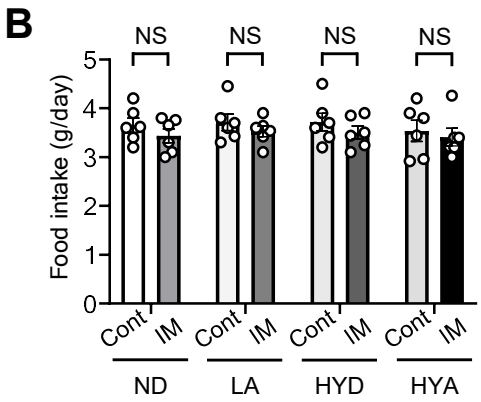

Figure S13. Prolonged limb immobilization by denervation influences the fecal levels of fatty acid metabolites produced by the gut microbiota

(A) Fatty acid concentrations in feces of control and denervated mice (10 days) (n = 6 mice). HYC was below the detection limit in all samples.

(B) Daily food intake of mice maintained on a normal diet (ND) or a diet containing LA, HYD, or HYA and subjected (or not) to cast-immobilization for 10 days (n = 6 mice).

Quantitative data are presented as means ± SEM (B) or medians with interquartile range (A). *$p < 0.05$, **$p < 0.01$, NS by the Mann-Whitney U test (A) or two-way ANOVA with the Bonferroni post hoc test (B).

Supplemental Figure 14

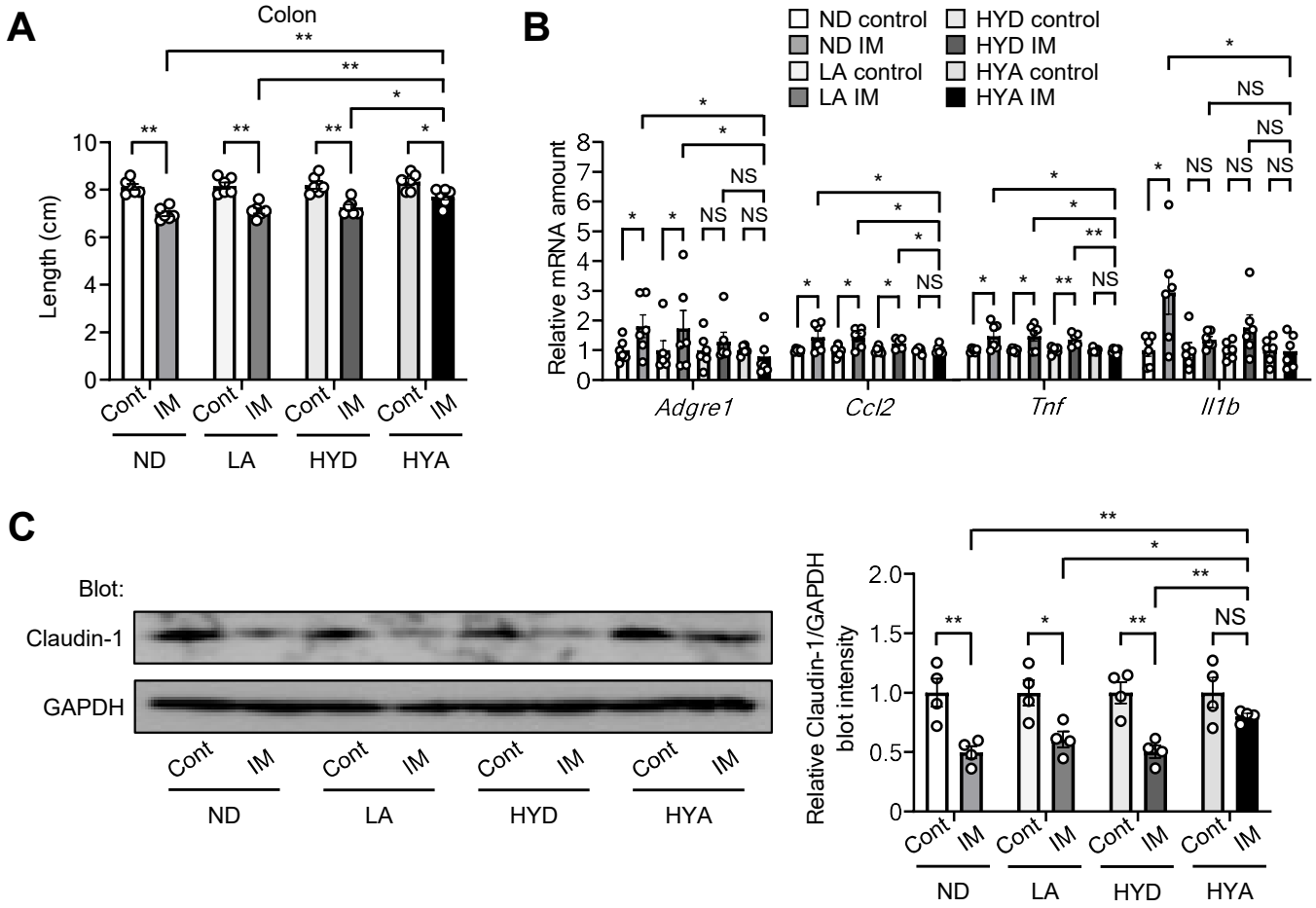

Figure S14. Effects of HYA on intestinal inflammation induced by prolonged limb immobilization

(A–C) Length of the colon (n = 6 mice) (A), RT-qPCR analysis of inflammation-related gene expression in the colon (n = 6 mice) (B), and immunoblot analysis of claudin-1 and GAPDH in the colon (n = 4 mice) (C) of mice fed a normal diet or a diet containing LA, HYD, or HYA and subjected (or not) to cast-immobilization for 10 days.

Quantitative data are presented as means ± SEM (A–C). *$p < 0.05$, **$p < 0.01$, NS by two-way ANOVA with the Bonferroni post hoc test.

Supplemental Figure 15

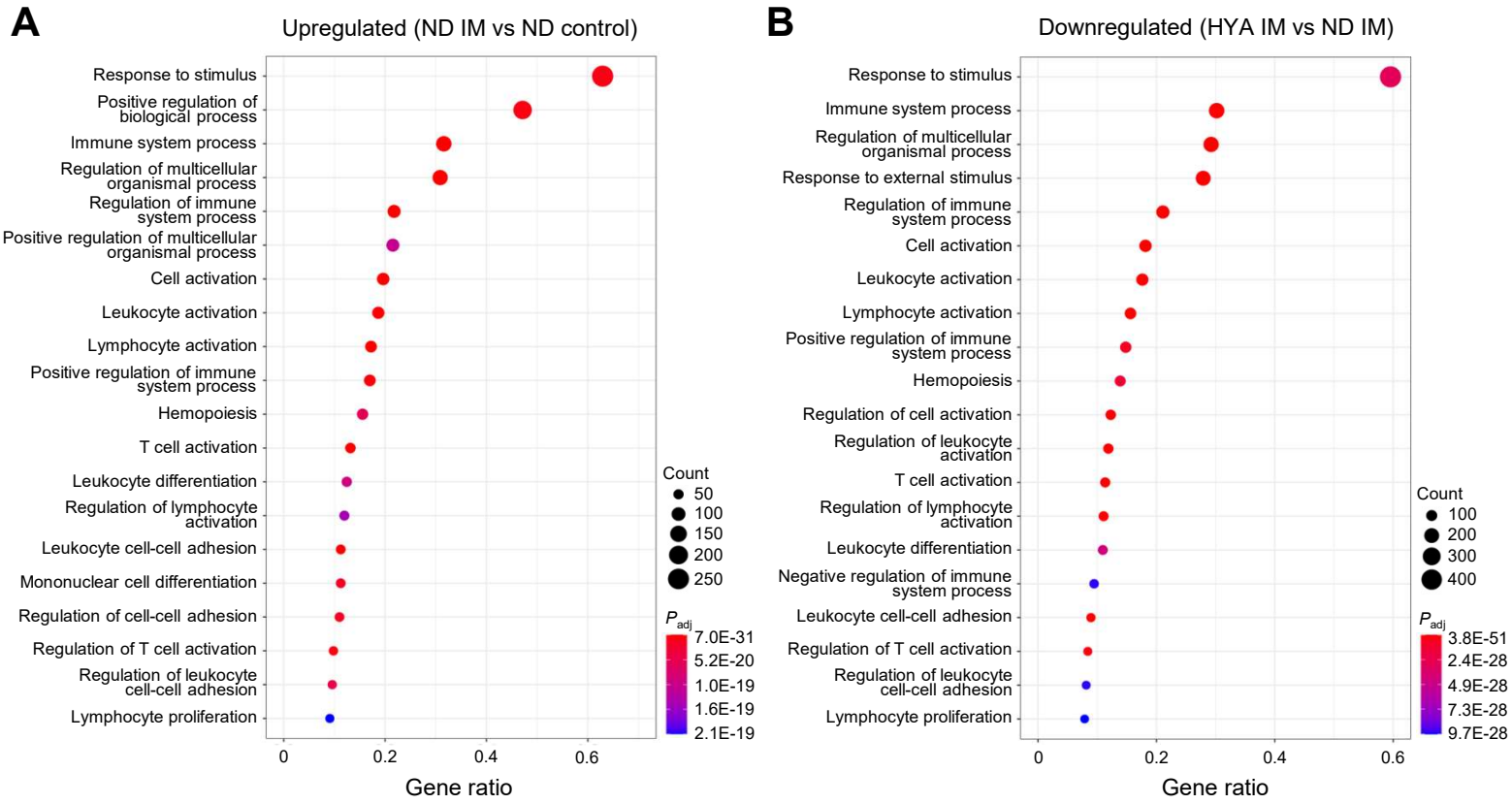

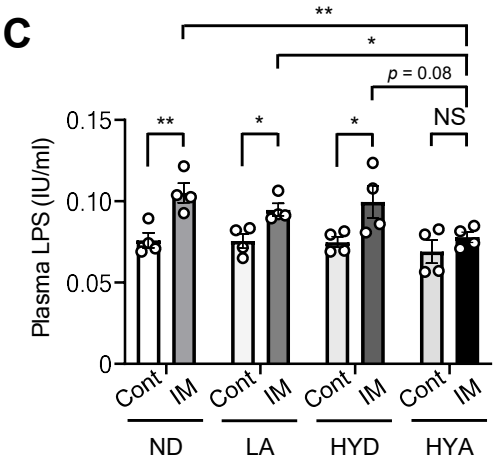

Figure S15. Effects of HYA on intestinal inflammation induced by prolonged limb immobilization

(A and B) GO functional analysis of RNA-seq data from the colon for biological processes upregulated in mice fed a normal diet and subjected to cast-immobilization for 10 days versus those not subjected to immobilization (A) as well as for biological processes downregulated in immobilized mice fed a diet containing HYA versus those fed a normal diet (B). The top 20 processes enriched among genes whose expression was altered by each condition are shown. p_{adj}, adjusted p value.

(C) Plasma concentration of LPS in mice fed a normal diet or a diet containing LA, HYD, or HYA and subjected (or not) to cast-immobilization for 10 days (n = 4 mice).

Quantitative data are presented as means ± SEM (C). *$p < 0.05$, **$p < 0.01$, NS by two-way ANOVA with the Bonferroni post hoc test.

Supplemental Figure 16

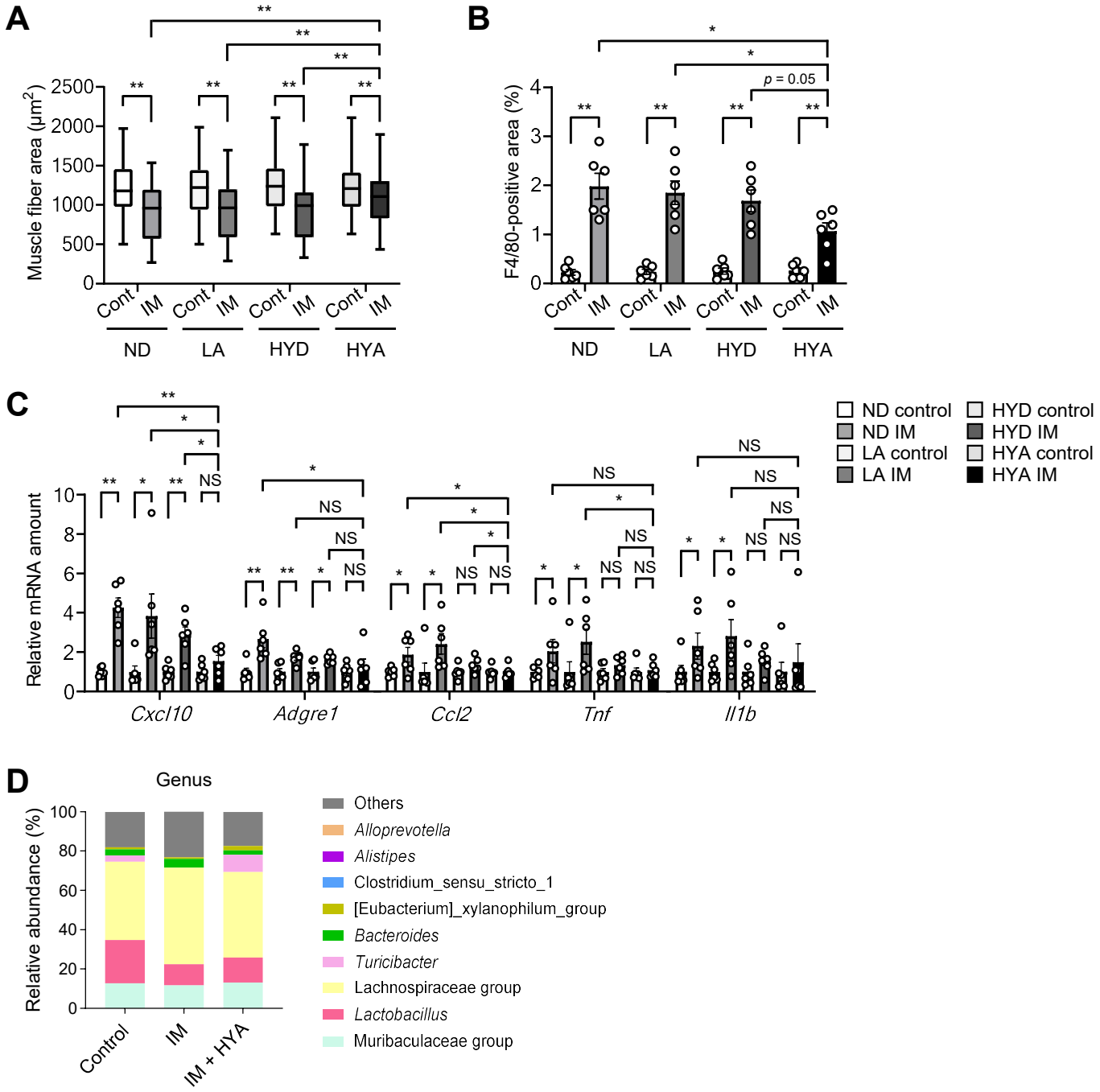

Figure S16. Effects of HYA on muscle inflammation and atrophy induced by prolonged limb immobilization

(A–C) Muscle fiber area (A) and the F4/80-positive area (B) in soleus (determined from images as in Figure 5E) as well as RT-qPCR analysis of inflammation-related gene expression in gastrocnemius (C) for mice fed a normal diet or a diet supplemented with LA, HYD, or HYA and subjected (or not) to cast-immobilization for 10 days (n = 6 mice). The area of 400 fibers pooled from four mice was measured and averaged for each condition in (A). (D) Gut microbial composition at the genus level for mice fed a normal diet or a diet containing HYA and subjected (or not) to cast-immobilization for 10 days (n = 4 mice). Quantitative data are presented as means ± SEM (B and C) or medians with interquartile range (A). *$p < 0.05$, **$p < 0.01$, NS by two-way ANOVA with the Bonferroni post hoc test.

Supplemental Figure 17

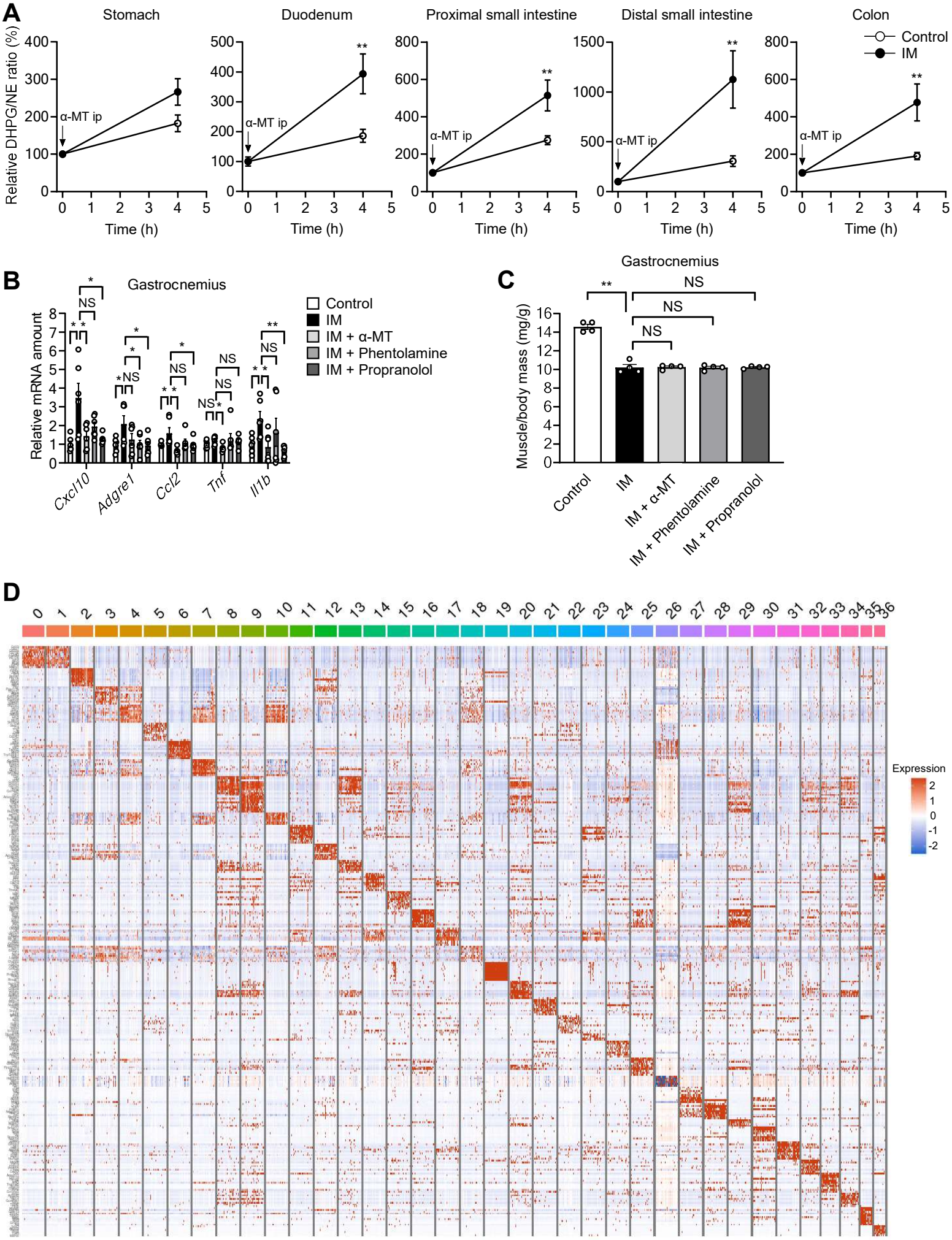

Figure S17. Sympathetic nerve activation contributes to muscle inflammation induced by limb immobilization

(A) Relative DHPG/NE ratio for the stomach, duodenum, proximal and distal small intestine, and colon of control or cast-immobilized (10 days) mice at 0 and 4 h after intraperitoneal (ip) injection of α-MT (n = 5 mice).

(B and C) RT-qPCR analysis of inflammation-related gene expression in gastrocnemius (n = 6 mice) (B) as well as the ratio of gastrocnemius muscle mass to body mass (n = 4 mice) (C) for mice subjected to intraperitoneal injection of α-MT, phentolamine, propranolol, or vehicle daily for 10 days with or without concomitant cast-immobilization.

(D) Heat map for the expression of all genes in the cell clusters of the colon identified by scRNA-seq analysis.

Quantitative data are presented as means ± SEM (A–C). *$p < 0.05$, **$p < 0.01$, NS by two-way ANOVA with the Bonferroni post hoc test.

Supplemental Figure 18

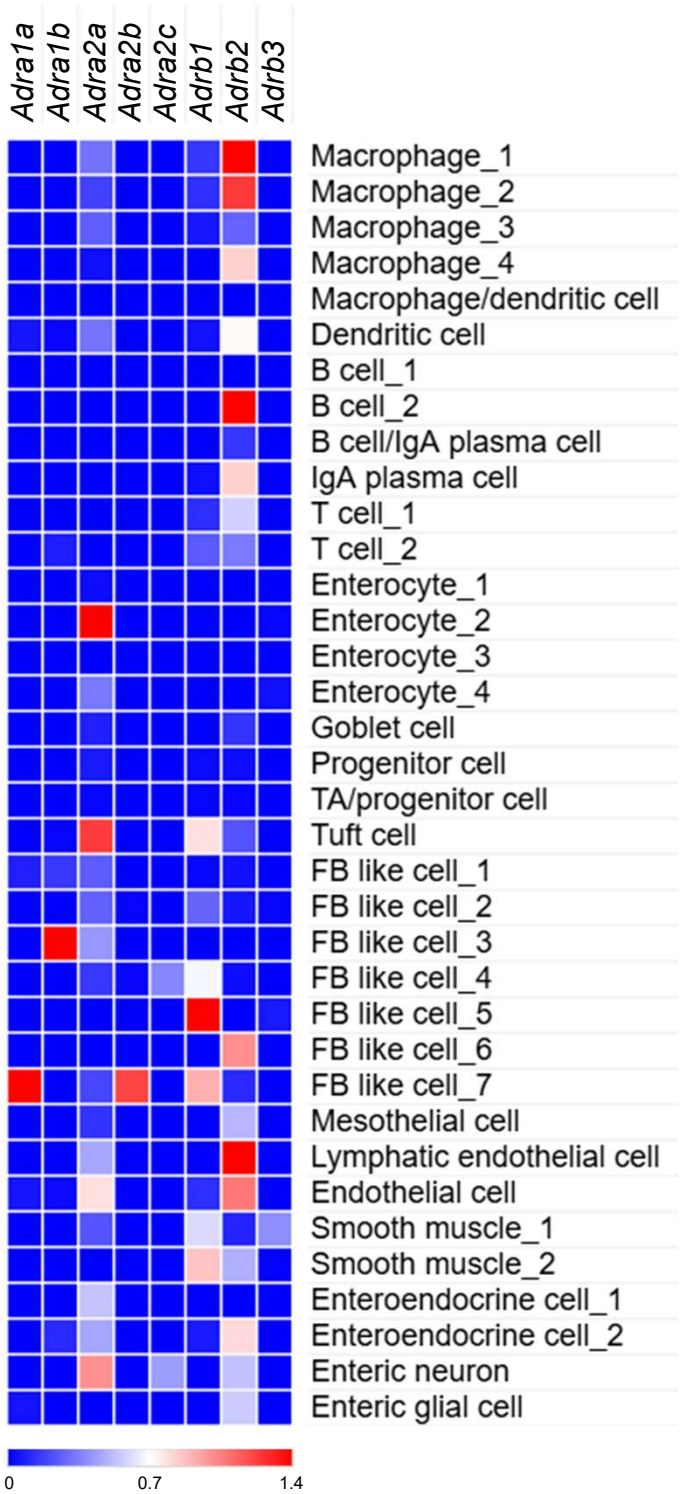

Figure S18. Heat map for expression of adrenergic receptor genes in cell clusters of the colon as determined by scRNA-seq analysis

Supplemental Figure 19

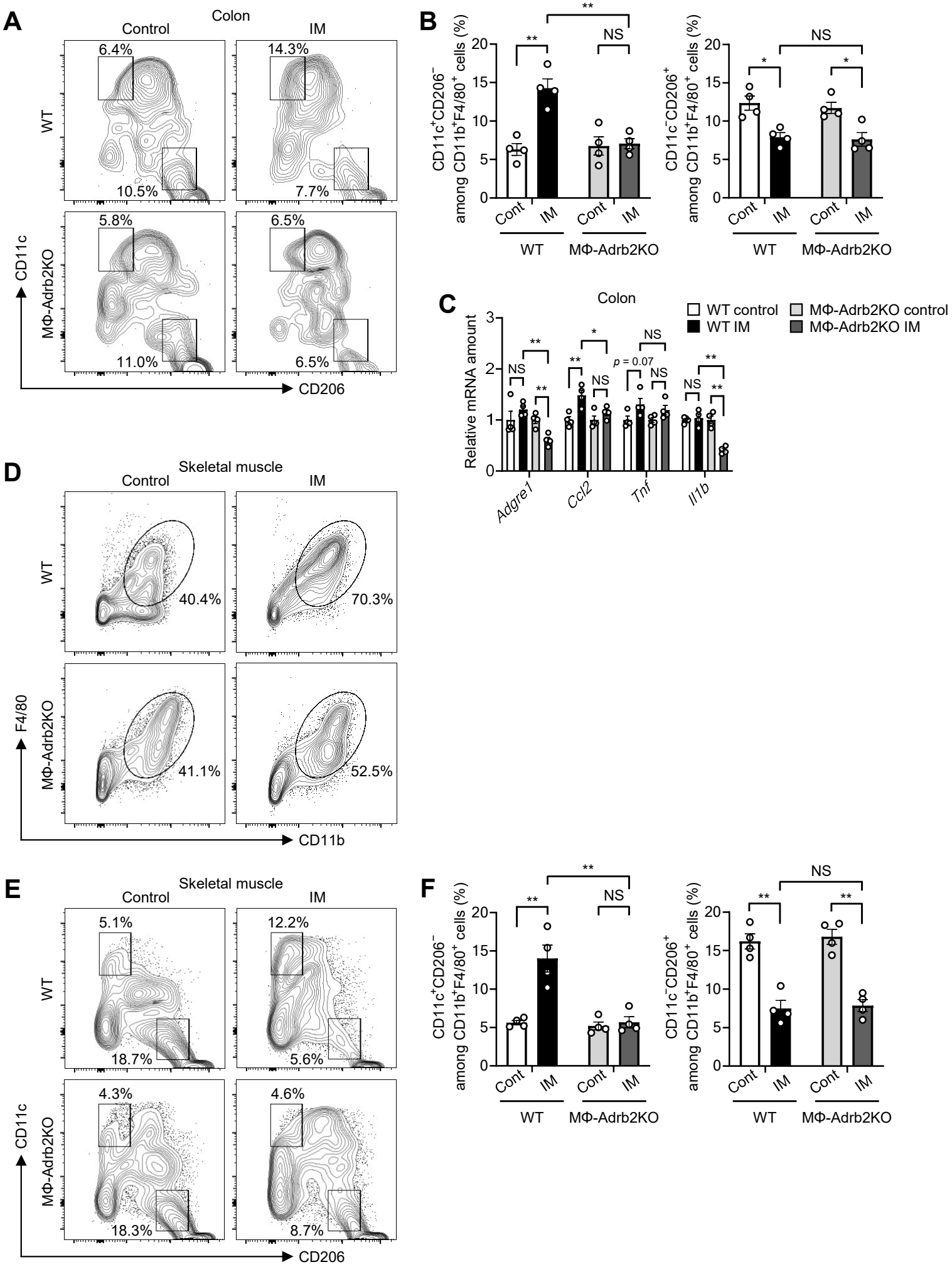

Figure S19. Intestinal and muscle inflammation induced by prolonged limb immobilization is attenuated in MΦ-Adrb2KO mice

(A–C) Representative flow cytometric analysis (A) and the percentage (B) of $CD11c^{+}CD206^{-}$ or $CD11c^{-}CD206^{+}$ cells among $CD11b^{+}F4/80^{+}$ cells as well as RT-qPCR analysis of inflammation-related gene expression (C) in the colon of WT or MΦ-Adrb2KO mice subjected (or not) to cast-immobilization for 10 days (n = 4 mice).

(D–F) Representative flow cytometric analysis of $CD11b^{+}F4/80^{+}$ cells among $CD45^{+}Ly6G^{-}$ cells (D) as well as representative flow cytometric analysis (E) and the percentage (F) of $CD11c^{+}CD206^{-}$ or $CD11c^{-}CD206^{+}$ cells among $CD11b^{+}F4/80^{+}$ cells in hind limb skeletal muscle of WT or MΦ-Adrb2KO mice subjected (or not) to cast immobilization for 10 days (n = 4 mice).

Quantitative data are presented as means ± SEM (B, C, and F). *$p < 0.05$, **$p < 0.01$, NS by two-way ANOVA with the Bonferroni post hoc test.

Supplemental Figure 20

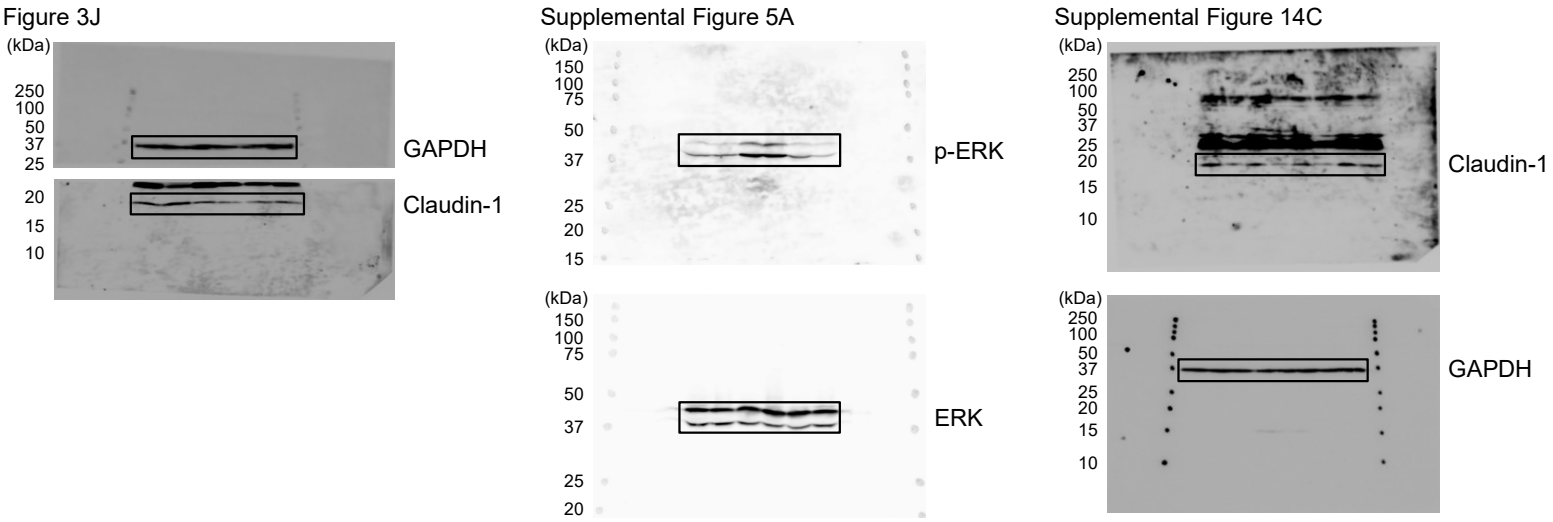

Figure S20. Uncropped immunoblot images
Black boxes contain the areas shown in the indicated figures.

Supplemental Table 1

Cluster	Key genes
Macrophage_1	*Cd68, Mrc1, Ctsa, Cd163*
Macrophage_2	*Itgam, Fcer1g, Mrc1, Retnla*
Macrophage_3	*Cd68, Fcer1g, Apoe, C1qb*
Macrophage_4	*Cd14, Itgam, Marco, Saa3*
Macrophage/dendritic cell	*Cd80, Cd86, Apol7c, Cacnb3*
Dendritic cell	*Itgax, Cd209a, Clec9a, Cst3*
B cell_1	*Cd19, Cd79a, Ighd, Ighm*
B cell_2	*Cd19, Cd79a, Ighd, Ighm*
B cell/IgA plasma cell	*Igha, Mzb1, Cd19*
IgA plasma cell	*Igha, Mzb1, Jchain*
T cell_1	*Cd3d, Cd8a, Cd4, Trac*
T cell_2	*Trbc1, Cd4, Id2, Il2ra*
Enterocyte_1	*Slc26a2, Aqp8, Slc20a1, Tgm3*
Enterocyte_2	*Slc26a2, Aqp8, Guca2a, Cyp2c55*
Enterocyte_3	*Slc26a2, Aqp8, Saa1, Car4*
Enterocyte_4	*Slc26a2, Slc26a3, Stard10, Fth1*
Goblet cell	*Tff3, Fcgbp, Clca1*
Progenitor cell	*Sox9, Cdk6, Muc4, Agr2*
TA/progenitor cell	*Ube2c, Sox9, Pigr, Ppp1r1b*
Tuft cell	*Trpm5, Pou2f3, Sh2d6*
FB like cell_1	*Col1a1, Fn1, Gsn, Dpt*
FB like cell_2	*Col1a1, Fn1, Ccn2, Adamdec1*
FB like cell_3	*Col1a1, Fn1, Pi16, Inmt*
FB like cell_4	*Col1a1, Fn1, Tnc, Sema3f*
FB like cell_5	*Fn1, Col1a2, Kit, Ano1*
FB like cell_6	*Col1a1, Col1a2, Clu, Mfge8*
FB like cell_7	*Col1a1, Col1a2, Jam2, Angptl2*
Mesothelial cell	*Msln, Wt1, C3, Slpi*
Lymphatic endothelial cell	*Lyve1, Pecam1, Ccl21a, Mmrn1*
Endothelial cell	*Pecam1, Vwf, Flt1, Egfl7*
Smooth muscle_1	*Des, Actg2, Acta2, Myh11*
Smooth muscle_2	*Actg2, Acta2, Hhip, Myh11*
Enteroendocrine cell_1	*Chga, Gcg, Pyy, Ins1*
Enteroendocrine cell_2	*Chga, Piezo2, Neurod1, Tph1*
Exocrine cell	*Ctrb1, Cela2a, Cela3b, Cpa1*
Enteric neuron	*Ncam1, L1cam, Tac1, Vip*
Enteric glial cell	*Gfap, Ncam1, L1cam, Adam11*

Table S1. Genes that characterize cell clusters of the colon identified by scRNA-seq analysis of control mice and mice subjected to cast-immobilization for 10 days

The exocrine cell cluster is characterized by expression of genes for digestive enzymes including *Ctrb1*, *Cela2a*, *Cela3b*, and *Cap1*, all of which are commonly expressed in pancreatic exocrine cells. Moreover, this cluster was detected in a specific sample. Given that this cluster may have been derived from ectopic pancreatic tissue congenitally admixed with intestinal tissue, or from contaminating pancreatic tissue artefactually introduced during intestinal tissue collection, it was excluded from further analysis.

Supplemental Table 2

Mouse gene	Primers (5' → 3')
36b4	FWD: GAGGAATCAGATGAGGATATGGGA
	REV: AAGCAGGCTGACTTGGTTGC
Adgre1	FWD: TGCCTCCCTGACTTTCAAAT
	REV: TGGCATTGCTGTATCTGCTC
Alt2	FWD: CAGACCCAGACAACATTTACCTG
	REV: CGCGGAGTACAAGGGATACTG
Bnip3	FWD: TTCCACTAGCACCTTCTGATGA
	REV: GAACACCGCATTTACAGAACAA
Ccl2	FWD: AGGTGTCCCAAAGAAGCTGTA
	REV: ATGTCTGGACCCATTCCTTCT
Cxcl10	FWD: TCCCTCTCGCAAGGAC
	REV: TTGGCTAAACGCTTTCAT
Fbxo32	FWD: GCAAACACTGCCACATTCTCTC
	REV: CTTGAGGGGAAAGTGAGACG
Foxo3a	FWD: CAGGCTCCTCACTGTATTCAGCTA
	REV: CATTGAACATGTCCAGGTCCAA
Il1b	FWD: GCTGAAAGCTCTCCACCTCA
	REV: AGGCCACAGGTATTTTGTCG
Klf15	FWD: ACCGAAATGCTCAGTGGGTTACCTA
	REV: GGAACAGAAGGCTTGCGAGTCA
Myh4	FWD: GAGCTACTGGATGCCAGTGAGCGC
	REV: CTGGACGATGTCTTCCATCTCTCC
Ptprc	FWD: ATGGTCCTCTGAATAAAGCCCA
	REV: TCAGCACTATTGGTAGGCTCC
Tnf	FWD: CATCTTCTCAAAATTCGAGTGACAA
	REV: TGGGAGTAGACAAGGTACAACCC
Trim63	FWD: GCTGGTGGAAAACATCATTGACAT
	REV: CATCGGGTGGCTGCCTTT

Table S2. Sequences of mouse primers for RT-qPCR analysis
FWD, forward; REV, reverse.

Supplemental Table 3

Human gene	Primers (5’ → 3’)
36B4	FWD: TTGTGGGAGCAGACAATGTG
	REV: TATTGGCCAGCAACATGTCC
ADGRE1	FWD: CCAGTGTTAATGCCGAAGTCT
	REV: GTGAACAGGTAAGCCATGACA
CCL2	FWD: CAGCCAGATGCAATCAATGCC
	REV: TGGAATCCTGAACCCACTTCT
CXCL10	FWD: TGCCATTCTGATTTGCTGCC
	REV: TGCAGGTACAGCGTACAGTT
IL1B	FWD: TTCGACACATGGGATAACGAGG
	REV: TTTTTGCTGTGAGTCCCGGAG
TNF	FWD: GAGGCCAAGCCCTGGTATG
	REV: CGGGCCGATTGATCTCAGC

Table S3. Sequences of human primers for RT-qPCR analysis
FWD, forward; REV, reverse.